Journal of Biomolecular NMR (2006) 36:79–102
DOI 10.1007/s10858-006-9047-4

Article

Quantifying Lipari–Szabo modelfree parameters from ^{13}CO NMR relaxation experiments

Tianzhi Wang[a,‡], Daniel S. Weaver[a], Sheng Cai[a,§] & Erik R. P. Zuiderweg[a,b,*]
[a]*Biophysics Research Division and* [b]*Departments of Biological Chemistry and Chemistry, University of Michigan, 930 N. University Avenue Ann Arbor, MI 48109-1055, USA*

Received 5 May 2006; Accepted 9 June 2006

Key words: calmodulin, computer software, order parameters, relaxation

Abstract

It is proposed to obtain effective Lipari–Szabo order parameters and local correlation times for relaxation vectors of protein ^{13}CO nuclei by carrying out a ^{13}CO-R_1 auto relaxation experiment, a transverse ^{13}CO CSA/^{13}CO – ^{13}Cα CSA/dipolar cross correlation and a transverse ^{13}CO CSA/^{13}CO–^{15}N CSA/dipolar cross correlation experiment. Given the global rotational correlation time from ^{15}N relaxation experiments, a new program COMFORD (CO-Modelfree Fitting Of Relaxation Data) is presented to fit the ^{13}CO data to an effective order parameter S^2_{CO}, an effective local correlation time and the orientation of the CSA tensor with respect to the molecular frame. It is shown that the effective S^2_{CO} is least sensitive to rotational fluctuations about an imaginary Cα – Cα axis and most sensitive to rotational fluctuations about an imaginary axis parallel to the NH bond direction. As such, the S^2_{CO} information is fully complementary to the ^{15}N relaxation order parameter, which is least sensitive to fluctuations about the NH axis and most sensitive to fluctuations about the Cα – Cα axis. The new paradigm is applied on data of Ca^{2+} saturated Calmodulin, and on available literature data for Ubiquitin. Our data indicate that the S^2_{CO} order parameters rapport on slower, and sometimes different, motions than the ^{15}N relaxation order parameters. The CO local correlation times correlate well with the calmodulin's secondary structure.

Abbreviations: COMFORD – CO modelfree fitting of relaxation data

The Lipari and Szabo spectral density function allows the dissection of NMR relaxation in terms of overall and local motion, characterized by modelfree order parameters and local correlation times in the nano-pico second time regime (Lipari and Szabo, 1982a, b). While not valid for all motional regimes, the description is intuitively clear and has as an advantage that theoretical motional models can be expressed in the same terms, allowing comparisons between experiment and theory (Lipari and Szabo, 1982a). The Lipari Szabo theory was first applied to NMR relaxation to extract dynamical information from a large number of ^{1}Hα-^{13}Cα R_1 and NOE relaxation vectors of cyclosporin A (Dellwo and Wand, 1989). Simultaneously, the protein NH relaxation protocol was introduced (Kay et al., 1989). Their protocol is almost synonymous with NMR protein

*To whom correspondence should be addressed. E-mail: zuiderwe@umich.edu
‡Present address: Department of Chemistry and Biochemistry, Auburn University, Auburn, AL 36849, USA.
§Present address: Division of Immunology, City of Hope National Medical Center, Duarte, CA 91010, USA.

backbone dynamics, and analyzes the three experiments ^{15}N R_1, R_2 and $\{^1H\}^{15}N$ NOE. An extended Lipari–Szabo protocol was introduced subsequently (Clore et al., 1990). Software packages such as NMRView for extraction of relaxation curves (Johnson and Blevins, 1994), and for obtaining the spectral density parameters of these data are available Modelfree (Mandel et al., 1995), Dasha (Orekhov et al., 1994) and TENSOR2 (Cordier et al., 1998). Wagner and co-workers showed that NH relaxation maybe interpreted in terms of spectral densities alone (Peng and Wagner, 1992a, b). The NH relaxation protocol has been extended to measurements of conformational changes at the milli–micro second time domain using relaxation dispersion in the rotating frame (Orekhov et al., 1994; Loria et al., 1999).

It is because of the many ^{15}N relaxation studies that one has obtained the *general* insight that entire proteins may be extremely rigid, completely floppy, or anywhere in between; it has changed the perspective on the rigidity of proteins in general. However, while the NH dynamics studies have been and will remain to be invaluable, it is obvious that complete dynamical characterization of a biomolecule can not be obtained from NH backbone dynamics alone. To extend the scope of experimental protein dynamics, Kay and co-workers developed ^2H methyl group relaxation methodology (Yang et al., 1998). These experiments showed that the dynamics of the methyl groups in SH2 domains are *not* quenched upon phospho-peptide binding, conceivably Nature's way to allow promiscuity in high-affinity ligand binding (Kay et al., 1998). In contrast, Wand and co-workers showed with these methods that an entropically costly quenching of methyl dynamics occurs upon peptide binding to calmodulin (Lee et al., 2000), conceivably disclosing Nature's way to allow high specificity in low affinity ligand binding. Methods to quantitatively measure and interpret ^1HN relaxation data have been developed by Torchia and co-workers, and disclosed important functional flap motions in the HIV protease (Ishima et al., 1999; 2004).

Several groups (Engelke and Ruterjans, 1997; Dayie and Wagner, 1997; Zuiderweg and co-workers, e.g. Zeng et al., 1996) introduced protein ^{13}CO spin-relaxation experiments to obtain additional probes on the dynamics of the protein backbone. Immediately, it was clear that the ^{13}CO experiments reveal a much larger dispersion in relaxation rates than the ^{15}N relaxation experiments. However, it was not known whether this dispersion was caused by a residue-to-residue variation of the ^{13}CO CSA tensor, which dominates the ^{13}CO relaxation at magnet fields above 14 T (600 MHz ^1H) or by a larger dispersion in local motions as detected by the ^{13}CO probes than the ^{15}NH probes. Even with those restrictions, the use of ^{13}CO dynamics experiments disclosed concerted motions of a helix in flavodoxin (Fischer et al., 1998), obtained better agreement between MD-calculated and NMR-detected order parameters for the loops of the enzyme binase (Pang et al., 2002), showed differences in the temperature dependence of ^{13}CO and ^{15}N detected dynamics (Wang et al., 2003), and demonstrated that ^{13}CO dynamics, in contrast to NH dynamics, detects a quenching of motions upon ligand binding to calmodulin (Lee et al., 2000; Wang et al., 2005). It is thus well established that it is worthwhile to obtain ^{13}CO relaxation data for a more complete description of the protein backbone dynamics, and for the associated entropic properties (Akke et al., 1993; Yang et al., 1997).

Recently, many open questions pertaining to the ^{13}CO CSA tensor in proteins have been answered. With high-level DFT calculations, it was shown that the ^{13}CO CSA tensor principal values σ_{11} and σ_{33} are constant within 7%, but that the σ_{22} value and tensor orientation is highly variable from site to site in proteins (Markwick and Sattler, 2004). These computational predictions confirmed earlier solid-state NMR data that related σ_{22} value variability to hydrogen bonding (Gu et al., 1994). The solid state NMR and theoretical findings were confirmed experimentally in solution by Bodenhausen and co-workers (Cisnetti et al., 2004; Loth et al., 2005). To do so, a set of 14 different auto- and cross-correlated relaxation experiments, involving both ^{15}N and ^{13}CO, was recorded and analyzed. The experimental and computational findings revealed that the variable σ_{22} can be obtained from

$$\sigma_{22} = 3\sigma_{iso} - \sigma_{11} - \sigma_{33} \quad (1)$$

with good precision.

Both theoretical and experimental work also showed that the σ_{11} and σ_{22} axes remain in the peptide plane for all residues, but that the orientation of σ_{11} can vary with an rms of 3.7 degrees with respect to the covalent bonds. The orientation

of the σ_{11} axis could not be correlated to any molecular parameter, and thus (for now) remains as the single unknown CSA parameter, variable from site-to-site.

Here, we propose to utilize these recent findings to obtain Lipari–Szabo order parameters, effective local correlation times and *the unknown orientation of the* ^{13}CO CSA σ_{11} axis for relaxation vectors of the ^{13}CO nucleus by carrying out three experiments: a ^{13}CO-R_1 auto relaxation experiment, a transverse ^{13}CO CSA/^{13}CO–^{13}Cα CSA/dipolar cross correlation ($\eta_{xy}^{CO,COC\alpha}$) and a transverse ^{13}CO CSA/^{13}CO-^{15}N CSA/dipolar cross correlation experiment ($\eta_{xy}^{CO,CON}$). These three experiments have in common that they are fully independent from the NH vector dynamics and are not affected by conformational broadening effects.

Given knowledge of τ_c (from ^{15}N R_1/R_2), we fit the data, on a residue-to-residue basis, to an effective order parameter S^2_{CO}, an effective local correlation time τ_{local} and the orientation of the ^{13}CO CSAσ_{11} axis with respect to the molecular frame. We show that the effective S^2_{CO} is least sensitive to fluctuations around an imaginary Cα – Cα axis (γ axis; Bremi and Bruschweiler, 1997) and most sensitive to motions around an imaginary axis parallel to the NH bond direction (the α axis). As such, the ^{13}CO relaxation information is fully complementary to the ^{15}N relaxation information, which is least sensitive to fluctuations around α and most sensitive to motions around γ (and β).

Our proposed approach is complementary to Chang and Tjandra's work, in which the ^{13}CO CSA tensor is determined and dynamical data obtained by carrying out R_1 and R_2 ^{13}CO relaxation experiments using up to four magnetic fields (Chang and Tjandra, 2005).

Theory

The goal of NMR relaxation studies is to extract from the raw relaxation rates spectral densities at nano to pico seconds which reflect the global and local dynamical events. While it is quite feasible to report such spectral densities without further interpretation (e.g. Peng and Wagner, 1992a, b; Farrow et al., 1995), we prefer to characterize the dynamics in terms of the Lipari–Szabo modelfree spectral density of the fluctuations of the magnetic vectors a and b (Lipari and Szabo, 1982a, b; Daragan and Mayo, 1996, 1997):

$$J^{ab}(\omega)=\frac{2}{5}\left\{\frac{S^{ab}\tau_c}{1+(\omega\tau_c)^2}+\frac{\left(P_2\left(\cos\theta^{ab}\right)-S^{ab}\right)\tau}{1+(\omega\tau)^2}\right\} \quad (2)$$

The fixed angle between the vectors a and b is denoted as θ^{ab} and

$$P_2\left(\cos\theta^{ab}\right)=(3\cos^2\theta^{ab}-1)/2. \quad (3)$$

When $a \equiv b$, the quantity S^{ab} is the familiar (squared) order parameter S^2; when $a \neq b$, S^{ab} is the cross-correlation order parameter. The inequality

$$(0 \leq |S^{ab}| \leq |P_2\left(\cos\theta^{ab}\right)|) \quad (4)$$

is valid for both cases. The correlation time τ_c affects both vectors a and b equally, i.e. equation (2) is only strictly valid for isotropic tumbling, while the time constant τ is given by

$$\tau=\frac{\tau_c\tau_{local}}{\tau_c+\tau_{local}} \quad (5)$$

where τ_{local} is the time constant that reflects an average of local motions affecting vectors a and b simultaneously. When $a \neq b$ this does *not* mean that vectors a and b are affected equally, as follows from the definition of the cross correlation order parameter:

$$S^{ab}=\frac{4\pi}{5}\sum_{m=-2}^{2}\langle Y_{2m}(\theta_a,\varphi_a)\rangle\left\langle Y^*_{2m}(\theta_b,\varphi_b)\right\rangle \quad (6)$$

The averages $\langle Y_{2m}(\theta_a,\varphi)\rangle$ and $\left\langle Y^*_{2m}(\theta_b,\varphi_b)\right\rangle$ depend on the local motion and are formally given by

$$\langle Y_{2m}(\theta_a,\varphi_a)\rangle=\frac{1}{4\pi}\int_0^{2\pi}\int_0^{\pi}Y_{2m}(\theta_a,\varphi_a)L_a(\theta_a,\varphi_a)\times\sin\theta_a d\theta_a d\varphi_a \quad (7)$$

where $L_a(\theta_a,\varphi_a)$ is the probability of finding interaction vector a at the local frame angles (θ_a,φ_a). The probability is dependent on the specific local motion and, for the same local motion, will generally affect vectors a and b differently, unless $a \equiv b$ or if it is a fluctuation around an axis lying in a plane bisecting the two vectors. Similar equations hold for vector b.

Our preference for describing local motions in terms of the Modelfree spectral density function

Figure 1. Theoretical dependency of the relaxation rates R_1^{CO} (green), $\eta_{xy}^{CO,COC\alpha}$ (red) and $\eta_{xy}^{CO,CON}$ (blue) on the CSA angle Θ, the local correlation time τ_{local} and the order parameter S^2_{CO}. The values $\sigma_{11} = 245$ ppm, $\sigma_{22} = 181$ ppm and $\sigma_{33} = 93$ ppm for the CO CSA (Loth et al., 2005) and $\tau_c = 7$ ns were used for each panel. a) Principal axis angle (Θ) dependence with $\tau_{local} = 70$ ps, $S^2_{CO} = 0.8$. b) Local correlation time (τ_{local}) dependence with $\Theta = 154°$ and $S^2_{CO} = 0.8$ c) Order parameter (S^2_{CO}) dependence with $\Theta = 154°$ and $\tau_{local} = 2$ ns (solid lines), $\tau_{local} = 100$ ps (dashed lines) and $\tau_{local} = 1$ ps (dotted lines).

derives from the fact that the effects of specific motional models can be computed from the equations [6] and [7], such as is carried out in Figure 5, and described in detail in the Supplementary material.

In the following, we assume that the overall correlation time τ_c is known from independent ^{15}N relaxation experiments. In addition, we temporarily assume, *until further discussion below*, that the local motion affecting the different ^{13}CO magnetic vectors is isotropic and can therefore be represented by a single order parameter S^2_{CO}. Then, a complete description of the two parameters, S^2_{CO} and τ_{loc} in the spectral density of equation (2) can be achieved if two independent relaxation measurements can be made, that are differently dependent on the (linear combinations) of spectral density functions. A classic choice would be to use the auto relaxation rates are R_1 and R_2. However, R_2 relaxation rates are often affected by chemical exchange processes (Ishima et al., 2004) which, when not suppressed, give rise to a third parameter, R_{ex}, to be fitted. The ^{13}CO R_1 relaxation can be obtained with sufficient sensitivity using extensions of the HNCO pulse sequence.

As will be shown below, the ^{13}CO R_1 relaxation rate (R_1^{CO}) is affected by many relaxation pathways, most of which have to be taken into account for analysis. A key contributor is the ^{13}CO CSA relaxation which can account for up to 70% of the R_1^{CO} relaxation rate. As mentioned in the Introduction, the ^{13}CO principal values σ_{11} and σ_{33} vary only little from residue to residue, allowing σ_{22} to be retrieved from the isotropic chemical shift. Hence, the ^{13}CO CSA tensor can be estimated to within 7% from the experimental data, and the overall R_1^{CO} relaxation rate is thus affected by variations of less than 5%, which is close to the achievable experimental uncertainty. Thus, we judge that the R_1^{CO} experiment is a suitable choice for quantitative ^{13}CO relaxation measurements. As a second ^{13}CO relaxation experiment, one could use the homonuclear $^{13}CO - {}^{13}C\alpha$ NOE experiment (Zheng et al., 1996). The experiment has as advantage that it solely dependent on the $^{13}CO - {}^{13}C\alpha$ dipolar interaction, dominated by the $J(0)$ term, but its sensitivity is, for smaller proteins, too low for quantitative evaluation on a residue-to-residue basis. However, its use in conjunction with other relaxation experiments will certainly be evaluated at a later stage.

Instead, we chose to use the ^{13}CO CSA/$^{13}CO - {}^{13}C\alpha$ transverse dipolar cross relaxation experiment ($\eta_{xy}^{CO,COC\alpha}$) (Fischer et al., 1997). For smaller proteins, these rates (the "^{13}CO TROSY effect") can be obtained readily from sensitive modified 3D HNCO experiments. However, as Figure 1a shows, these rates are, in addition to the sought-after dynamic parameters, very sensitive to the variations in orientation of the CSA principal axes with respect to the COCα bond vector, which are known to occur from theoretical and experimental work (Markwick and Sattler, 2004; Loth et al., 2005).

Hence, the $CO - C\alpha$ cross correlation experiment introduces one additional site-to-site variable, Θ. Fortunately, Θ can be obtained by using yet another cross correlation experiment that is dependent on the same parameters, but which "looks at" the CSA tensor from a different angle (Pang and Zuiderweg, 2000). The experiment of choice is the ^{13}CO CSA/^{13}CO–^{15}N transverse dipolar cross correlation ($\eta_{xy}^{CO,CON}$) (Ghose et al., 1998). As shown in Figure 1a, the Θ dependences of $\eta_{xy}^{CO,CON}$ and $\eta_{xy}^{CO,COC\alpha}$ are anti-correlated. Obviously, and as shown in Figure 1a, the R_1^{CO} rate is independent of the orientation of the CSA tensor. We elect to *not* use the transverse cross correlation rate $\eta_{xy}^{CO,CO-HN}$ (Pang and Zuiderweg, 2000) since we now know that this rate is affected by (unknown) variations in the ^{13}CO–^{1}H^{15}N vector orientation and direction due to dynamical N pyramidalization (Palmo et al., 2003; Mannfors et al., 2003).

In summary, we propose here to obtain Lipari–Szabo spectral density function parameters for dynamical processes on the pico-nano second time scale for the ^{13}CO nucleus using R_1^{CO}, $\eta_{xy}^{CO,COC\alpha}$ and $\eta_{xy}^{CO,CON}$. Together with ^{15}N relaxation

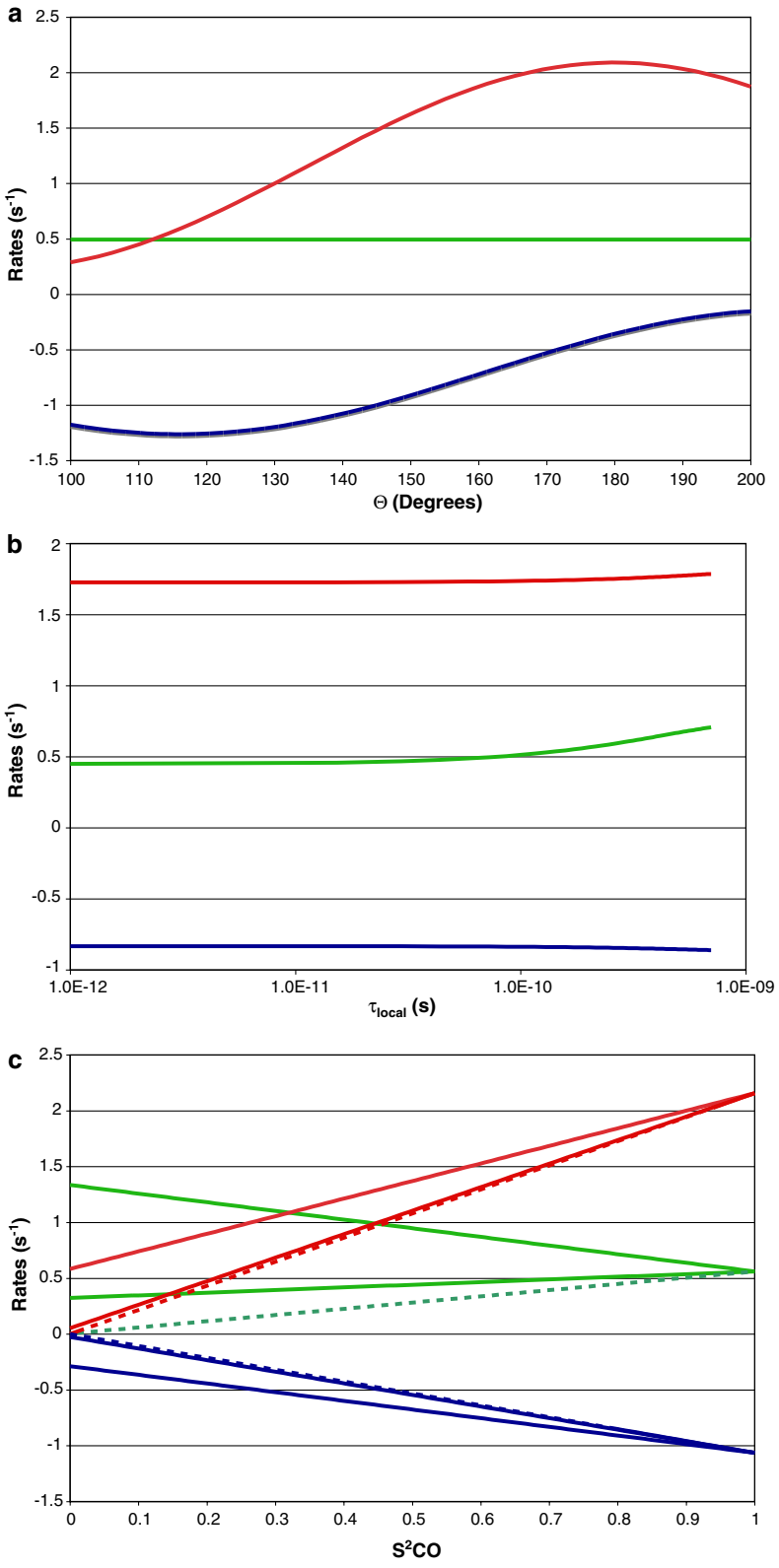
a
Rates (s-1)
2.5
2
1.5
1
0.5
0
-0.5
-1
-1.5
100
110
120
130
140
150
160
170
180
190
200
Θ (Degrees)
b
Rates (s-1)
2
1.5
1
0.5
0
-0.5
-1
1.0E-12
1.0E-11
1.0E-10
1.0E-09
τlocal (s)
c
Rates (s-1)
2.5
2
1.5
1
0.5
0
-0.5
-1
-1.5
0
0.1
0.2
0.3
0.4
0.5
0.6
0.7
0.8
0.9
1
S2CO

measurements that provide an initial estimate for the overall τ_c, the experiments can be used to determine three independent parameters, i.e. S^2_{CO}, τ_{loc} and the angle Θ describing the direction of the ^{13}CO CSA tensor principal axis with respect to the $^{13}CO-^{13}C\alpha$ vector. Alternatively, the data could also be used to obtain values of the spectral density functions $J(\omega_C), J(2\omega_C)$ and the angle Θ.

The R_1^{CO} relaxation rate for proteated proteins including all terms that contribute 1% or more, is given by (Fischer et al., 1998b):

$$\begin{aligned}R_1^{CO}=&\frac{1}{8}\left[\left(\frac{\mu_0}{4\pi}\right)\frac{\hbar\gamma_C\gamma_C}{r^3_{CO-Ca}}\right]^2*\{2J(\omega_{C-C})+6J(\omega_C)\\&+12J(\omega_{C+C})\}+\sum_{k=Ca,Cb,CO}\frac{1}{8}\left[\left(\frac{\mu_0}{4\pi}\right)\frac{\hbar\gamma_C\gamma_C}{r^3_{CO-Ck}}\right]^2\\&*\{2J(\omega_{C-C})+6J(\omega_C)+12J(\omega_{C+C})\}\\&+\frac{1}{8}\left[\left(\frac{\mu_0}{4\pi}\right)\frac{\hbar\gamma_C\gamma_N}{r^3_{CO-N}}\right]^2*\{2J(\omega_{C-N})+6J(\omega_C)\\&+12J(\omega_{C+N})\}+\sum_{HN,Ha}\frac{1}{8}\left[\left(\frac{\mu_0}{4\pi}\right)\frac{\hbar\gamma_C\gamma_H}{r^3_{CO-H}}\right]^2\\&*\{2J(\omega_{H-C})+6J(\omega_C)+12J(\omega_{H+C})\}\\&+\sum_{l=Ha,Hb}\frac{1}{8}\left[\left(\frac{\mu_0}{4\pi}\right)\frac{\hbar\gamma_C\gamma_H}{r^3_{CO-Hl}}\right]^2*\{2J(\omega_{H-C})\\&+6J(\omega_C)+12J(\omega_{H+C})\}\\&+\frac{1}{18}(\gamma_C B_0)^2*\Delta\sigma^2\\&*\left[1+\frac{1}{3}\left(\frac{\sigma_{22}-\sigma_{33}}{\sigma_{11}-\sigma_{iso}}\right)^2\right]*6J(\omega_C)\end{aligned}\tag{8}$$

where $\Delta\sigma$ and σ_{iso} are given by

$$\Delta\sigma=\sigma_{11}-\frac{\sigma_{22}-\sigma_{33}}{2}\tag{9}$$

and

$$\sigma_{iso}=\frac{\sigma_{11}+\sigma_{22}+\sigma_{33}}{3}\tag{10}$$

and where the sum k over the ^{13}C relaxation partners includes $C\alpha(i+1)$(at 2.4Å) $C\beta$(at 3Å) and $CO(i-1)$ (at 3 Å). Protons that contribute to the ^{13}CO relaxation are HN *(i+1)* (at 2.10 Å) and $H\alpha$*(i)* (at 2.20 Å) and $H\beta(i)$ and $H\alpha$*(i+1)* all at 3 Å. The latter protons can be replaced by deuterons, in which case they do not contribute to the R_1 relaxation. CSA relaxation accounts for about 70% of the total while a multitude of dipolar relaxation processes contribute the other 30%. However, the dipolar R_1^{CO} relaxation is dominated by the $^{13}CO-^{13}C\alpha$ dipolar relaxation, because it is in turn dominated by the zero quantum term $J(\omega_{CO-C\alpha})$, which is numerically indistinguishable to the $J(0)$ spectral density. Thus, the ^{13}CO relaxation can be qualitatively understood in terms of $^{13}CO-^{13}C\alpha$ dipolar relaxation and the ^{13}CO CSA relaxation. For perdeuterated proteins, the dominance of the of $^{13}CO-^{13}C\alpha$ dipolar relaxation and the ^{13}CO CSA relaxation is larger.

The transverse $^{13}CO-CSA$ $^{13}CO-^{13}C\alpha$ dipolar cross correlation rate, $\eta_{xy}^{CO,COC\alpha}$ for a rhombic ^{13}CO CSA tensor is given by (Goldman, 1984):

$$\eta_{xy}^{CO,COC\alpha}=\frac{1}{6}\left(\frac{\mu_0}{4\pi}\right)\frac{\hbar\omega_c\gamma_c\gamma_c}{r^3_{CO-C\alpha}}*\left\{\begin{array}{c}(\sigma_{11}-\sigma_{33})\{4J^{11,CO-C\alpha}(0)+3J^{11,CO-C\alpha}(\omega_c)\}\\+(\sigma_{22}-\sigma_{33})\{4J^{22,CO-C\alpha}(0)+3J^{22,CO-C\alpha}(\omega_c)\}\end{array}\right\}\tag{11}$$

where the Lipari–Szabo cross correlation spectral density functions are given by equation (2), in which the angles θ^{ab} are between the principal axes σ_{11} or σ_{22} of the CSA tensor of ^{13}CO and the $^{13}CO-^{13}C\alpha$ dipolar interaction vector (see inset of Figure 5). The angles differ, trivially, by 90 degrees. Similarly, the transverse ^{13}CO-CSA ^{13}CO–^{15}N dipolar cross correlation rate, $\eta_{xy}^{CO,CON}$ is given by

$$\eta_{xy}^{CO,CON}=\frac{1}{6}\left(\frac{\mu_0}{4\pi}\right)\frac{\hbar\omega_c\gamma_c\gamma_N}{r^3_{CO-N}}*\left\{\begin{array}{c}(\sigma_{11}-\sigma_{33})\{4J^{11,CO-N}(0)+3J^{11,CO-N}(\omega_c)\}\\+(\sigma_{22}-\sigma_{33})\{4J^{22,CO-N}(0)+3J^{22,CO-N}(\omega_c)\}\end{array}\right\}\tag{12}$$

The interaction angles $\theta^{ii,CO-C\alpha}$ relevant to equation (11) differ from angles $\theta^{ii,CO-N}$ in equation (12) by the Cα–CO–N bond angle of 117 degrees since σ_{11} and σ_{22} both lie in the peptide plane.

Figure 1 a, b and c shows the dependency of the R_1^{CO} rate and the cross correlation rates on the different parameters in the equations. It is clearly seen that the R_1^{CO} rate is not sensitive to the angle Θ, (Figure 1a) but is sensitive to local motion at the mid-frequency range, predominantly due to the ω_c dependency of the CSA auto relaxation

(Figure 1b); the change in rates is 53% over the range shown. As indicated above, the cross correlation rates $\eta_{xy}^{CO,COC\alpha}$ and $\eta_{xy}^{CO,COC\alpha}$ are very dependent on the angle Θ, but are in contrast, hardly affected by the local correlation time (see Figure 1b): the rate changes are only 3% over the range shown. All rates are, of course, dependent on the order parameter (Figure 1c). However, while the cross correlation rates decrease monotonously with the order parameter S^2, the R_1^{CO} rate can both decrease or increase with decreasing order parameter, depending whether the local correlation time τ_{loc} is fast or slow with respect to ω_c. This property is unique, and makes the R_1^{CO} rate determination very valuable for extracting local order parameters. The explorations of parameter space thus show that the three measures R_1^{CO}, $\eta_{xy}^{CO,COC\alpha}$ and $\eta_{xy}^{CO,COC\alpha}$ have very different dependencies on the underlying motional (S^2 and τ_{loc}) and structural (Θ) parameters, which makes them an ideal choice for the measurement of these parameters.

Materials and methods

NMR experiments

All experiments were carried out with uniformly $^{15}N/^{13}C$ labeled Chicken Calmodulin (Ca^{2+}-CaM) obtained from Dr. A. J. Wand (University of Pennsylvania) and described in detail elsewhere (Urbauer et al., 1995). The 500 µl NMR sample contained about 1 mM in 0.02% sodium azide, 100 mM KCl, 5.5 mM total $CaCl_2$ concentration, 10 mM imidazole-d_4, 90% H_2O/10% D_2O in pH 6.5. The NMR experiments were performed on a Bruker Avance 500 (regular triple resonance probe) and a Bruker Avance 600 MHz NMR spectrometer (triple resonance cryo-probe) at 35°C.

^{15}N relaxation rate measurements

The spin-lattice relaxation rate ^{15}N-R_1, spin-spin relaxation rate ^{15}N-R_2 (CPMG) and ^{15}N NOE were measured on Bruker Avance 500 MHz spectrometer at 35°C. The sequences used were slightly modified from those published (Tjandra et al., 1996). The main difference is that half as many ^1H π pulses as usual are delivered during the ^{15}N CPMG sequence, allowing a faster repetition rate (4 kHz) of the ^{15}N π pulses to better suppress conformational exchange broadening effects (Wang et al., 2003). The ^1H carrier was set to the frequency of the water resonance, and the ^{15}N carrier was set to 118 ppm. Each two-dimensional data set contained $2k \times 128$ complex points, with spectral widths of 7,002 and 1,562 Hz for the ^1H and ^{15}N dimensions, respectively. States-TPPI quadrature detection in the t_1 dimension was used. The relaxation delays were 10, 30, 50, 100, 150, 200, 250, 350, 400, 450 and 500 ms and 6, 12, 24, 35, 59, 70, 94, 118, 130 and 141 ms for R_1 and R_2 respectively. The length of the proton saturation for NOE measurements was 4 s. The NOE control experiments were collected with a 4 s recycle delay, and the water magnetization was kept on +z throughout.

^{13}CO longitudinal relaxation rate measurements

The ^{13}CO T_1 (R_1^{CO}) experiment was carried out on a Bruker Avance 600 MHz instrument at 35°C. The HNCO-type pulse sequence previously developed (Zheng et al., 1996) was slightly modified to completely saturate the water signal at all times though purge and crusher pulses (see the discussion below). The experiments were collected as two-dimensional data sets containing $2k \times 40$ complex points, with spectral widths of 12,019 and 1,500 Hz for the ^1H and ^{13}CO dimensions, respectively. The experiments were recorded with 48 scans each, with 11 relaxation delays (80*2, 240, 400, 560, 640*2, 800, 960*2, 1120, and 1280 ms) in 24 h total.

$^{13}CO - ^{13}C_\alpha$ cross-correlated relaxation rate measurements

Transverse $^{13}CO(CSA)/^{13}CO - ^{13}C_\alpha$ ($\eta_{xy}^{CO,COC\alpha}$) and $^{13}CO(CSA)/^{13}CO–^{15}N$ ($\eta_{xy}^{CO,CON}$) cross-correlated relaxation rates between ^{13}CO chemical shift anisotropy and the $^{13}CO-^{13}C_\alpha$ or $^{13}CO-^{15}N$ dipolar interaction were measured on a Bruker Avance 600 MHz instrument at 35°C. Modified 3D HNCO experiments were used without $^{13}C_\alpha$ or ^{15}N decoupling during a constant-time ^{13}CO evolution time, as illustrated in Figure 2. For calmodulin, these simple experiments are nearly twice as sensitive as the elegant symmetric reconversion experiments (Loth et al., 2005), since they donot contain refocussing delays. The CT evolution time, which doubles as the cross-correlated relaxation delay, was 54 or 80 ms (N*1/2 $J_{C'C\alpha}$ and N*1/2 $J_{C'N}$ respectively). As has been described previously (Fischer et al., 1997), these experiments measure purely single-exponential decays of the

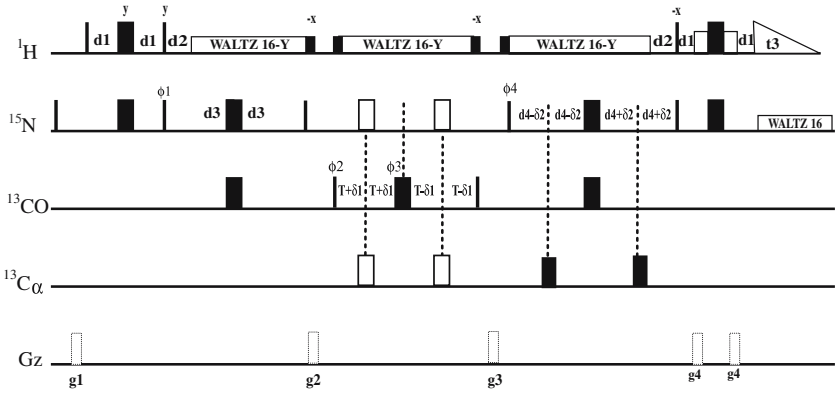

Figure 2. Pulse scheme of the $\eta_{xy}^{CO,COC\alpha}$ and $\eta_{xy}^{CO,CON}$ transverse cross-correlated relaxation rate experiments. Narrow and thin bars represent 90° and 180° pulses, respectively. Unless specified otherwise, pulse phases are along the x-axis. ^{1}H, ^{15}N, ^{13}CO and $^{13}C\alpha$ carriers are positioned at 4.8, 118, 175 and 55 ppm, respectively. All ^{13}C rectangular 90° and 180° pulses have durations of $\sqrt{15}/4\Delta$ and $\sqrt{3}/4\Delta$ respectively, where Δ is the difference in Hz between the center of the ^{13}CO and $^{13}C\alpha$ chemical shift. The half-sinebell shaped pulse field gradients used are: $g1$ = (40 G/cm, 1 ms), $g2$ = (30 G/cm, 1 ms), $g3$ = (60 G/cm, 1 ms), $g4$ = (50 G/cm, 1 ms), and $g5$ = (50 G/cm, 1 ms). The WATERGATE scheme was used to suppress the solvent resonance. In the $\eta_{xy}^{CO,COC\alpha}$ experiment, 4T = 54 ms while the two open 180° ^{15}N decoupling pulses are issued, but not the two open 180 $^{13}C\alpha$ pulses. For the $\eta_{xy}^{CO,CON}$ experiment 4T = 80 ms, the two open 180° $^{13}C\alpha$ decoupling pulses are issued, but not the two open 180° ^{15}N pulses. Phase cycle: $\phi1$ = x, −x; $\phi2$ = x, x, −x, −x; $\phi3$ = x, x, x, x, −x, −x, −x, −x, y, y, y, y, −y, −y, −y, −y; $\phi4$ = x, x, x, x; rec = x, −x, −x, x, x, −x, −x, x, −x, x, x, −x, −x, x, x, −x. States-TPPI quadrature detection in F1 and F2 is achieved by incrementing $\phi2$ and $\phi4$, respectively. The indirect sampling times were $t_1 = 4 * \delta_1$ and $t_2 = 4 * \delta_2$.

cross correlated relaxation eigenstates. Each three-dimensional data set contained $2k \times 80 \times 28$ or $2k \times 120 \times 28$ complex points for ^{1}H, ^{13}C, ^{15}N, with spectral widths of 12,019, 1,500 and 1,824 Hz for the ^{1}H, ^{13}CO and ^{15}N dimensions, respectively. The ^{1}H carrier was set to the frequency of the water resonance, the ^{15}N carrier was set to 118 ppm and the ^{13}CO carrier was set to 176 ppm. Each 3D experiment was recorded with 16 scans for a total experimental time of 48 ($\eta_{xy}^{CO,COC\alpha}$) or 72 h ($\eta_{xy}^{CO,CON}$).

Fitting the $\eta_{xy}^{CO,COC\alpha}$ *and* $\eta_{xy}^{CO,CON}$ *cross correlation rates*

The NMR experiments in Figure 2 yield three dimensional in-phase HNCO cross peaks with $^{13}CO - {}^{13}C\alpha$ or $^{13}CO - {}^{15}N$ doublet structure. The ^{13}CO evolution, which doubles as the cross correlation relaxation period, is constant time. The time domain data is processed as follows using NMRPipe (Delaglio et al., 1995): weighing and Fourier transform (Ft) of the ^{1}H (t_3) dimension; Ft of the ^{13}CO dimension (t_1) without window functions and retaining both the real and imaginary transforms; mirror-image linear prediction, weighing and Ft of the ^{15}N dimension (t_2); and finally, an inverse Ft of the ^{13}CO dimension.

We use a home-written FORTRAN-77 program to extract the ^{13}CO constant-time interferograms from the obtained complex $(\omega_1, t_2*, \omega_3)$ NMRPipe matrix. Typically, we co-add a block of 5×5 CO interferograms centered on the HN position of the HNCO cross peak to increase signal to noise and to capture both CO doublet peaks, which are slightly offset from each other because of $^{1}H^{15}N - {}^{13}C\alpha$ and $^{15}N - {}^{13}C\alpha$ scalar coupling (E-COSY) effects. For Calmodulin the 3D spectrum was sufficiently resolved to be able to extract 120 ^{13}CO interferograms that contained only a single doublet.

The intensities of the two doublet components in the interferograms were obtained with a FORTRAN-77 program using a target function containing two (for $\eta_{xy}^{CO,CON}$) or three cosines (for $\eta_{xy}^{CO,COC\alpha}$), with frequencies and intensities as fitting parameters (Figure 3a). A general inhomogeneous linebroadening (decay) was included in the fitting and was found to be 0.86 Hz. The program follows a simulated annealing protocol. A third minor component, restrained to be centered between the doublet peaks, was found to be necessary for the best fitting of the $\eta_{xy}^{CO,COC\alpha}$ data. This component, which varies between 0 and 10%, accounts for partial $^{13}CO - {}^{13}C\alpha$ decoupling, caused by imperfections in the selective ^{13}CO and

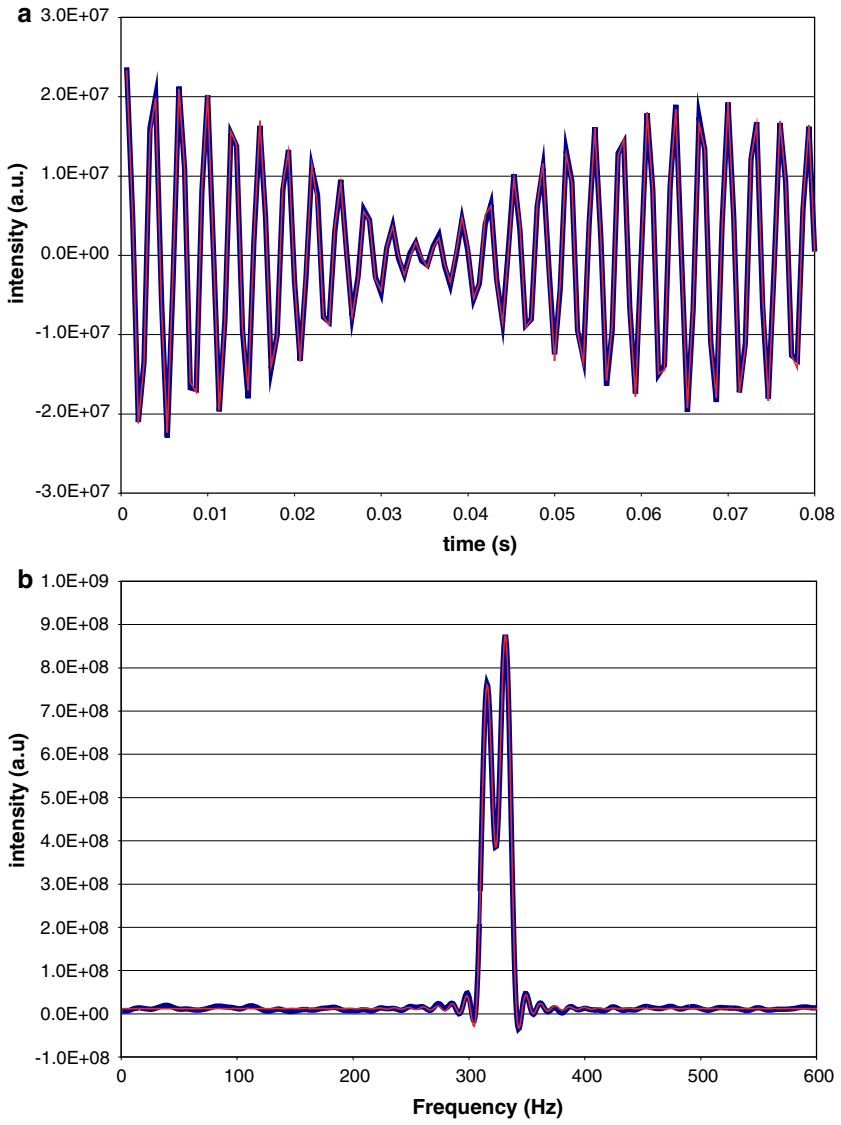

Figure 3. Representative signal to noise ratio in the $\eta_{xy}^{CO,CON}$ experiment, quality of time domain fitting of the interferogram, and overlay of the resulting weighed Fourier transformed spectra. The data was extracted out of the 3D HNCO matrix, in which the ^{15}N-coupled ^{13}CO-dimension has been retained in the (complex) time domain (Figure 3a). The fitting was carried out using 2 non-decaying complex cosines with their intensity and frequency as variables. A general inhomogeneous broadening was fitted as well (panel a, blue: experimental ^{13}CO-dimension interferogram; red, fitted). While irrelevant for parameter extraction, the resulting experimental and fitted interferograms were Fourier transformed with identical window functions and overlaid for visual inspection of the quality of the fit (panel b, blue: experimental ^{13}CO-dimension spectrum; red, fitted).

$^{13}C\alpha$ pulses in the t_2 time domain. Errors of fit were estimated using a Monte-Carlo routine. Typical errors of fit for the amplitudes were 0.5%. The final fit was further inspected for quality by comparing the Fourier transformed fit with the Fourier transform of the extracted experimental interferogram, using identical window functions, shown in Figure 3b.

The cross correlation rates $\eta_{xy}^{CO,COC\alpha}$ are subsequently obtained from the equation

$$\eta_{xy}^{CO,COC\alpha} = \frac{1}{2T}\ln\left(\frac{I_{CO}^{C\alpha\uparrow}}{I_{CO}^{C\alpha\downarrow}}\right) \qquad (13)$$

where T is the constant relaxation time, and $I_{CO}^{C\alpha\uparrow}$ and $I_{CO}^{C\alpha\downarrow}$ are the intensities of the doublet components as

obtained from the time-domain fittingprocedure. Analogous equations hold for $\eta_{xy}^{CO,CON}$.

The errors $\Delta\eta$ in the rate fitting parameters η were obtained using:

$$\Delta\eta = \frac{1}{2T}\sqrt{\left(\frac{1}{I_{CO}^{C\alpha\uparrow}}\Delta I_{CO}^{C\alpha\uparrow}\right)^2 + \left(\frac{1}{I_{CO}^{C\alpha\downarrow}}\Delta I_{CO}^{C\alpha\downarrow}\right)^2} \tag{14}$$

where $\Delta I_{CO}^{C\alpha\uparrow}$ and $\Delta I_{CO}^{C\alpha\downarrow}$ correspond the uncertainties in the intensities of the fitted doublet components (typically 1–2%). The R_1^{CO} relaxation rate was fitted from the experimental data using a single exponential in the program NMR view (Johnson and Blevins, 1994). The error in the fitted data was obtained from the program.

Fitting of the relaxation rates to motional parameters

We wrote a FORTRAN-77 program COMFORD (CO-Modelfree Fitting Of Relaxation Data) that fits simultaneously the R_1^{CO}, $\eta_{xy}^{CO,COC\alpha}$ and $\eta_{xy}^{CO,CON}$ relaxation rates. COMFORD uses as additional input the ^{13}CO isotropic shift and an overall correlation time. Typically, τ_c is obtained from ^{15}N relaxation experiments, but can also be obtained iteratively with the COMFORD program by optimizing the best global fit. In the case of calmodulin, we obtained a τ_c of 6.9 ns for the N-terminal globular section (1–79) and a τ_c of 6.5 ns for the C-terminal globular section (80–148), in agreement with the values obtained from ^{15}N relaxation (Wang et al., 2005). The current version of COMFORD does not yet allow for global anisotropic tumbling.

COMFORD carries out a three-dimensional grid search for the parameter S_{CO}^2 over the range {0.01–1.0} in linear steps of 0.01; τ_{local} over the range {1 ps to $\tau_c/10$} in geometric steps of 1.1 and Θ over the range {120–200°} in linear steps of 1°. COMFORD accepts and records as solution any combination of these parameters for which

$$\sqrt{\left(\frac{\left(R_1^{calc}-R_1^{exp}\right)^2}{\sigma_{R1}^2} + \frac{\left(\eta_{xy,CO-C\alpha}^{calc}-\eta_{xy,CO-C\alpha}^{exp}\right)^2}{\sigma_{\eta xy,CO-C\alpha}^2} + \frac{\left(\eta_{xy,CO-N}^{calc}-\eta_{xy,CO-N}^{exp}\right)^2}{\sigma_{\eta xy,CO-N}^2}\right)} \le \sqrt{3} \tag{15}$$

where the calculated rates are obtained using equations (8), (10) and (12) and where the factors σ are the experimental uncertainties. The program uses $\sigma_{11} = 245$ ppm and $\sigma_{33} = 93$ ppm, as obtained by (Loth et al., 2005), keeps τ_c constant, and computes the values of σ_{22} from the isotropic chemical shift according to equation (1).

For each experimental data point $\{R_1^{exp}, \eta_{xy,CO-C\alpha}^{exp}, \eta_{xy,CO-N}^{exp}\}$, COMFORD carries out additional grid searches for the six combinations

$$\left\{R_1^{exp} \pm \sigma_{R1}, \eta_{xy,CO-C\alpha}^{exp}, \eta_{xy,CO-N}^{exp}\right\},$$
$$\left\{R_1^{exp}, \eta_{xy,CO-C\alpha}^{exp} \pm \sigma_{\eta xy,CO-C\alpha}, \eta_{xy,CO-N}^{exp}\right\},$$
$$\left\{R_1^{exp}, \eta_{xy,CO-C\alpha}^{exp}, \eta_{xy,CO-N}^{exp} \pm \sigma_{\eta xy,CO-N}\right\},$$

the twelve combinations

$$\left\{R_1^{exp}, \eta_{xy,CO-C\alpha}^{exp} \pm \sigma_{\eta xy,CO-C\alpha}\sqrt{2}, \eta_{xy,CO-N}^{exp} \pm \sigma_{\eta xy,CO-N}\sqrt{2}\right\},$$
$$\left\{R_1^{exp} \pm \sigma_{R1}\sqrt{2}, \eta_{xy,CO-C\alpha}^{exp}, \eta_{xy,CO-N}^{exp} \pm \sigma_{\eta xy,CO-N}\sqrt{2}\right\},$$
$$\left\{R_1^{exp} \pm \sigma_{R1}\sqrt{2}, \eta_{xy,CO-C\alpha}^{exp} \pm \sigma_{\eta xy,CO-C\alpha}\sqrt{2}, \eta_{xy,CO-N}^{exp}\right\},$$

and the eight combinations $\{R_1^{exp} \pm \sigma_{R1}\sqrt{3}, \eta_{xy,CO-C\alpha}^{exp} \pm \sigma_{\eta xy,CO-C\alpha}\sqrt{3}, \eta_{xy,CO-N}^{exp} \pm \sigma_{\eta xy,\,CO-N}\sqrt{3}\}$, for a total of 27 searches. All acceptable solutions (''hits'') for these searches are tallied in a three-dimensional histogram of the parameter S_{CO}^2, τ_{local} and Θ all with the same ranges and steps as the search itself.

For each residue, the fitted values of the parameters S_{CO}^2, τ_{local} and Θ are read from the histogram element with the largest number of ''hits''. The reported fitting errors in the parameters S_{CO}^2, τ_{local} and theta are obtained from the

histogram elements that have half the largest number of "hits", on either side of the maximum, and independently for the three parameters. The histograms are reset to zero when the program moves to the next residue.

COMFORD yielded the best convergence at the known overall rotational correlation times of the two domains of CaM (6.9 and 6.5 ns, respectively) and Ubiquitin (4.15 ns) using the distances $d_{CO-C\alpha} = 1.50$Å and $d_{CO\text{-}N} = 1.32$ Å, both within the limits as observed for these lengths in the high-resolution X-ray structure of Crambin (1.50–1.55 Å and 1.30–1.35 Å respectively, Jelsch et al., 2000).

A complete COMFORD calculation for the 105 residues of calmodulin including error ranges, takes about 4 hours of CPU time on a 1.25 GHz Macintosh G4 Powerbook. The program has a flag to work with data from either proteated or per-deuterated proteins. All FORTRAN-77 source codes quoted are available from the corresponding author.

Other data

We also fitted the three relevant ^{13}CO relaxation rates for ^{15}N, ^{13}C, ^{2}H labeled ubiquitin at 303 K from the data provided in the supplementary materials by (Loth et al., 2005). COMFORD converged best at a correlation time of 4.15 ns, which is very close to what we have obtained (3.95 ns) for the same protein from earlier ^{15}N relaxation studies in our lab (Wang et al., 2003).

Results and discussion

Our group has long promoted the use of ^{13}CO-relaxation data in order to obtain NMR relaxation and mobility data on the backbone from other vectors than just the HN dipolar pair (Zheng et al., 1996; Fischer et al., 1997, 1998a, b; Pang et al., 2002) After initial investigations, it became quite clear that the ^{13}CO relaxation is dependent on several more parameters than just mobility; hence, in recent years we have used ^{13}CO relaxation data to describe only *average* dynamic behavior. Recently, the variability of the ^{13}CO tensor parameters was parameterized (Cisnetti et al., 2004; Loth et al., 2005). The ^{13}CO CSA tensor principal values σ_{11} and σ_{33} are constant within 7%, but the σ_{22} value is highly variable from site to site, but can be obtained from $\sigma_{22} = 3\sigma_{iso} - \sigma_{11} - \sigma_{33}$. They also show that the σ_{11} direction can vary by 17 degrees in the peptide plane. The only unknown structural parameter thus is given by the angle Θ describing the σ_{11} direction with respect to the COCα axis. Hence, it now possible to use ^{13}CO relaxation data, and deconvolute the tensorial and motional components associated with equations [8], [10] and [12] using the program COMFORD.

NMR experimentation

Cross correlated NMR experiments are very robust, because they measure the *difference or ratio* of the relaxation behavior of two relaxation components – hence, even if the relaxation rates themselves may be compromised by conformational exchange and/or a multitude of mechanisms, the cross correlated rates are reliable. We use the experiment described in Figure 2 that yields resolved doublet components rather than a symmetric reconversion approach (Loth et al., 2005). The reasons are as follows. Taking each of the 4 reconversion experiments to represent unit sensitivity, our experiment has 50% relative sensitivity because it separates the C'X doublet components. However, we can run it with 4 times the number of transients in the same overall experimental time, giving the same overall sensitivity. With these premises, numerical simulations show that both experiments yield accurate cross-correlation data, with equal precision given a certain experimental error (the final error in the computed cross-correlation rates is about 5 times the error in the raw data). However, the symmetric reconversions are based on refocussing and development of the $2C_+N_z$ antiphase coherences (59 ms) while the experiment in Figure 2 is not. For Calmodulin with $\tau_c = 7.0$ ns and an average R^2_{CO} of 10 s^{-1} at 600 MHz, this (re) focusing causes a 45% sensitivity loss. Overall thus, our doublet experiment contains the cross correlation rates at about twice the precision per unit experimental time. However, this gain comes at a cost: the challenge is to properly quantitate the data. First of all, the data have to be recorded as a 3D rather than a 2D dataset in order to cleanly separate the doublet components. The price is $1/\sqrt{2}$ in sensitivity. Second, we have found that we can not have confidence in the amplitudes of the cross correla-

tion doublets in the frequency domain because the scalar coupling $^{13}CO - {}^{13}C\alpha$, and even more, the $^{13}CO-{}^{15}N$ scalar coupling is not large enough to provide a clean separation of the doublet components as compared to the (CSA relaxation dominated) ^{13}CO line width. Hence, we find it much more reliable to laboriously fit the ^{13}CO (constant) time domain data. We carry this out with a program that fits the amplitudes and frequencies of in-phase cosines as described in the Materials and Methods. Figure 3a shows the quality of the time domain fits against the constant-time interferograms, while Figure 3b demonstrates how well the experimental and fitted frequency domain data correspond.

The R_1^{CO} relaxation data can be obtained relatively rapidly using the pulse sequence of (Zhang et al., 1996). For the molecule studied, Calmodulin, it was sufficient to use a 2D version of the experiment. To obtain the true R_1^{CO} relaxation rate, one needs to suppress both cross relaxation and cross correlation effects. Therefore, the R_1^{CO} relaxation period must contain $^{13}C\alpha$ decoupling pulses (suppressing both $^{13}CO - {}^{13}C\alpha$ NOE and $\eta_z^{CO,COC\alpha}$ cross correlation), ^{15}N π pulses (suppressing $\eta_z^{CO,CON}$ cross correlation) and ^{1}H π pulses (suppressing ^{1}H–^{13}CO NOE). The increasing number of ^{1}H pulses in an increasing R_1^{CO} relaxation period will progressively saturate the ^{1}H magnetization, and the H_2O magnetization in particular. Hence, any attempts to keep the water signal ''up'' will progressively fail when the ^{13}CO relaxation time and number of ^{1}H pulses increase. This will lead to an artificially fast ^{13}CO relaxation rate of those ^{13}CO's that are measured through the amide protons that exchange fast with solvent. Hence, we saturate the solvent resonance at all times (using purge and crusher pulses,) to create a consistent initial condition to the R_1^{CO} relaxation experiment.

Quality of the COMFORD fit

COMFORD obtains, per residue, the best values of the fitting parameters S^2_{CO}, τ_{local} and Θ by carrying out a grid search. It carries out an estimation of the propagation of experimental error into the fitted parameters by fitting 27 combinations of the experimental data R_1, $\eta_{xy}^{CO,COC\alpha}$ and $\eta_{xy}^{CO,CON}$ and their respective experimental uncertainties. In this way, COMFORD obtains the deepest and widest range of the fitting parameters S^2_{CO}, τ_{local} and Θ that correspond to the experimental ranges of R_1 $\eta_{xy}^{CO,COC\alpha}$ and $\eta_{xy}^{CO,COC\alpha}$. This approach obtains the best ''free energy'' fit (the area with most solutions) rather than a best ''lowest energy'' (the one best solution) fit. This approach was necessary, since we observed that the best ''lowest energy'' point, obtained from a minimization procedure, may indeed not correspond with the global free energy minimum. We like the assurance of the grid search that the obtained fitted parameters must correspond to the best solution and that nothing was missed. Computationally, the grid search procedure is not much slower than a simulated annealing approach.

Figure 4(a–d) show the performance of COMFORD using calculated input data for a proteated protein, $\tau_c = 10$ ns at 14.6 T (600 MHz ^{1}H), with all 60 combinations of $S^2_{CO} = 0.1, 0.3, 0.5, 0.7$ and 0.9, $\tau_{local} = 50, 658, 1450$ and 2030 ps and $\Theta = 135, 155$ and 175 degrees. The input data were modified with random errors, corresponding to 2% rmse on R_1, 3% rmse on $\eta_{xy}^{CO,COC\alpha}$ and 4% rmse $\eta_{xy}^{CO,CON}$. The fits to the input rates, shown in Figure 4a, are excellent. Figure 4(b–d) show contour plots of the obtained order parameters, local correlation times and tensor angles for the 60 cases. One appreciates that the certain combinations for the input rates give rise to multiple solutions, especially for the local correlation times, lesser so for the order parameters and not for the angles. Strong bifurcation in solutions is observed for a local correlation time input value of 658 ps, with the majority of the solutions ending up at 2700 ps. In the other cases, the majority of the solutions are at, or close to, the input values. The latter is also the case for the order parameters. In these cases, the program reports the parameter with the highest occurrence.

That certain rate input parameters are compatible with multiple values of the spectral density parameters of equation (2) is not a problem unique to COMFORD. As shown in Figure 5, such degeneracy is inherent to the mathematical shape of the Lipari–Szabo function, where two sets of parameters give rise to indistinguishable spectral density values over a large range that includes the ^{13}C (and ^{15}N) frequencies of most NMR spectrometers. Similar multiple-mimina problems have been analyzed in conjunction with ^{15}N relaxation experiments (Levy et al., 1981; Andrec et al., 1999; d'Auvergne and Gooley, 2003). It speaks to the

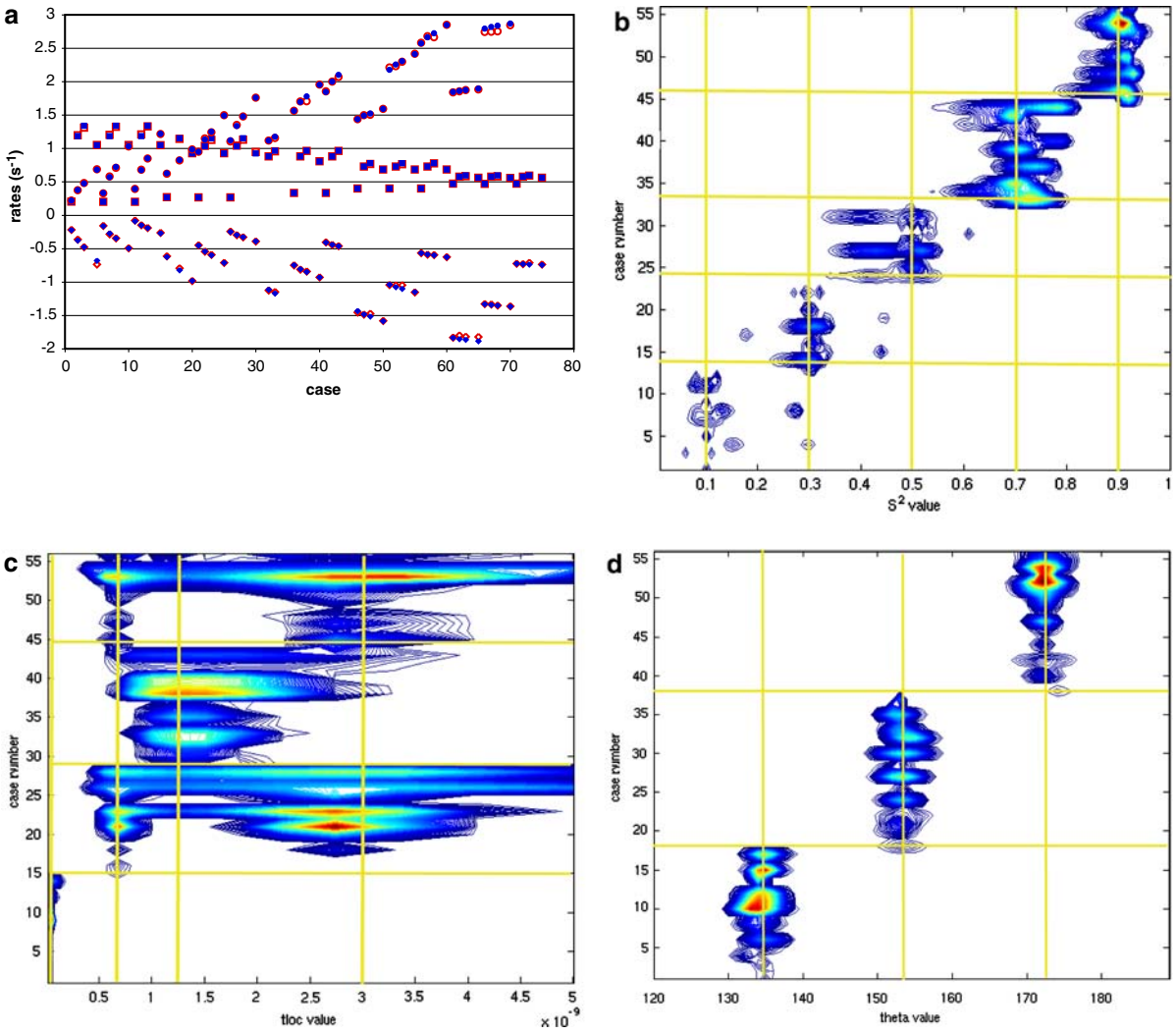

Figure 4. Test-fits of COMFORD on computed R_1^{CO}, $\eta_{xy}^{CO,COC\alpha}$ and $\eta_{xy}^{CO,CON}$ input, with $\tau_c = 10$ ns at 14.6 T (600 MHz ^{1}H), with 60 combinations of $S^2_{CO} = 0.1$, 0.3, 0.5, 0.7 and 0.9, $\tau_{local} = 50$, 658, 1450 and 2030 ps and $\theta = 135$, 155 and 175 degrees. The input data were modified with random errors, corresponding to 2% rmse on R_1^{CO}, 3% rmse on $\eta_{xy}^{CO,COC\alpha}$ and 4% rmse $\eta_{xy}^{CO,CON}$. Panel a. The input and fitted $\eta_{xy}^{CO,COC\alpha}$ are in closed blue and open red *circles* respectively. The input and fitted R_1^{CO} are in closed blue and open red *squares* respectively. The input and fitted $\eta_{xy}^{CO,CON}$ are in closed blue and open red *diamonds* respectively. Panel b. Contour plot of the S^2_{CO} solutions to the computed input (case numbers). For instance, for each of the 60 values S^2_{CO}, τ_{local} and θ, 27 fits are computed corresponding to the input rates +/- the input errors, as described above. For each of these, the program tracks and stores every grid search point for which the error of fit is satisfied (see equation (15)). The number of "hits" in the S^2_{CO} contour plot varies between 0 and 730 per grid point. The horizontal yellow lines separate cases with different input order parameters, from 0.1, 0.3, 0.5, 0.7 and 0.9, from bottom to top. The vertical yellow lines indicate the target values. Panel c. Contour plot of the τ_{local} solutions to the computed input (case numbers). The number of "hits" in the τ_{local} contour plot varies between 0 and 700 per grid point. The horizontal yellow lines separate cases with different input parameters, from $\tau_{local} = 50$, 658, 1450 and 2030 ps, from bottom to top. The vertical yellow lines indicate the target values. Panel d. Contour plot of the θ_1 solutions to the computed input (case numbers). The number of "hits" in the θ_1 contour plot varies between 0 and 900 per grid point. The horizontal yellow lines separate cases with different input parameters, from $\theta = 135$, 155 and 175 degrees, from bottom to top. The vertical yellow lines indicate the target values.

quality of the COMFORD grid search algorithm that such bifurcations are indeed obtained. COMFORD does provide for these contour plots as a standard output. It is recommended that they are checked for bifurcations before the Lipari–Szabo parameters are reported.

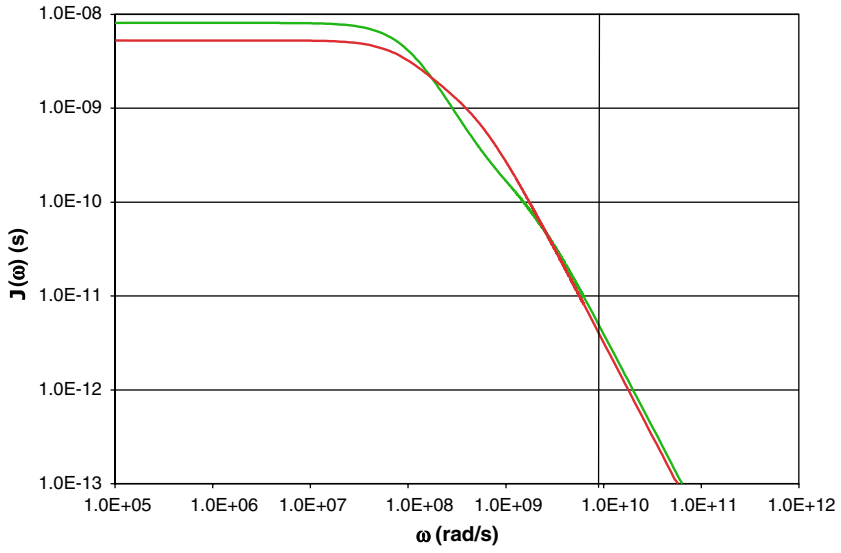

Figure 5. Plots of the Lipari–Szabo spectral density function for the values $\tau_c = 10$ ns, $\tau_{local} = 658$ ps and $S^2 = 0.80$ (green) and $\tau_c = 10$ ns, $\tau_{local} = 2700$ ps and $S^2 = 0.40$ (red). The ^{13}C frequency at 14.6 T (600 MHz ^1H) is indicated with a vertical line.

Figure 6a shows the raw relaxation rates for residues 1–80 Calmodulin and their fitting using our program COMFORD that optimizes the target function given in equation (15). The quality of the fit is excellent: of the 56 residues for which complete data was available, 47 converged to within the value $X = \sqrt{3}$ or better (see Table 1). We find that good fits can *only* be obtained with the values of σ_{11} and σ_{33} as reported from the literature, d_{COCA} of 1.50 Å, and values of τ_c as found from ^{15}N relaxation experiments. Change of any of these parameters results in significantly worse fits (not shown).

We proceeded by asking whether convergence can also be obtained when one of three parameters is kept fixed. When Θ is kept constant at the average value found for the normal fit, a value of 154° (corresponding to an angle β between the σ_{11} axis and the C'N bond of 37°) we can fit only 26 out of 56 residues, while the quality of the fit for these residues is much worse, (Table 1). Hence, the computation strongly supports that Θ cannot be constant, and varies from residue to residue. In contrast, fixing the value for σ_{22} does not affect the fitting procedure much, if at all (not shown).

Next, we questioned whether the variation in the raw relaxation rates data could be fitted by variations of the angle Θ and τ_{local} only, while keeping the order parameter constant (at an average 0.76). The results of this try are not good either (Table 1). Neither is the fit when the local correlation time τ_{local} is kept fixed at the average value of 510 ps found from the complete fit, an extreme fast time of 52 ps or at the maximum allowed value of 690 ps (see Table 1). The latter fit (or rather, lack thereof) is shown in Figure 6b.

The combined results of fixing the order parameter and local correlation time are thus unsatisfactory, and demonstrate clearly that the ^{13}CO relaxation data on calmodulin contains dynamic information.

Figure 6. Quality of the COMFORD fit versus the experimental relaxation data of residues 1–80 of Ca^{2+}-saturated Calmodulin (600 MHz). For all panels, the experimental and fitted $\eta_{xy}^{CO,COC\alpha}$ are in blue and red *circles* respectively. The experimental and fitted R_1^{CO} are in blue and red *squares* respectively. The experimental and fitted $\eta_{xy}^{CO,CON}$ are in blue and red *diamonds* respectively. The values $\sigma_{11} = 245$ ppm, and $\sigma_{33} = 93$ ppm for the ^{13}CO CSA and $\tau_c = 6.9$ ns are the same in each panel. The values of σ_{22} were obtained from $\sigma_{22} = \sigma_{iso} * 3 - \sigma_{11} - \sigma_{33}$ a) The fit versus the experimental relaxation data optimizing S^2_{CO}, τ_{loc} and the angle Θ between the ^{13}CO CSA tensor principal axis σ_{11} and the CO – Cα bond vector. b) The fit versus the experimental relaxation data optimizing S^2_{CO} and Θ when using a constant value for τ_{local} of 690 ps. c) The fit versus the experimental relaxation data optimizing S^2_{CO}, τ_{loc} and the distance $^{13}CO - {}^{13}C\alpha$ in the range 1.50–1.55 Å, when using a constant angle Θ of 154 degrees.

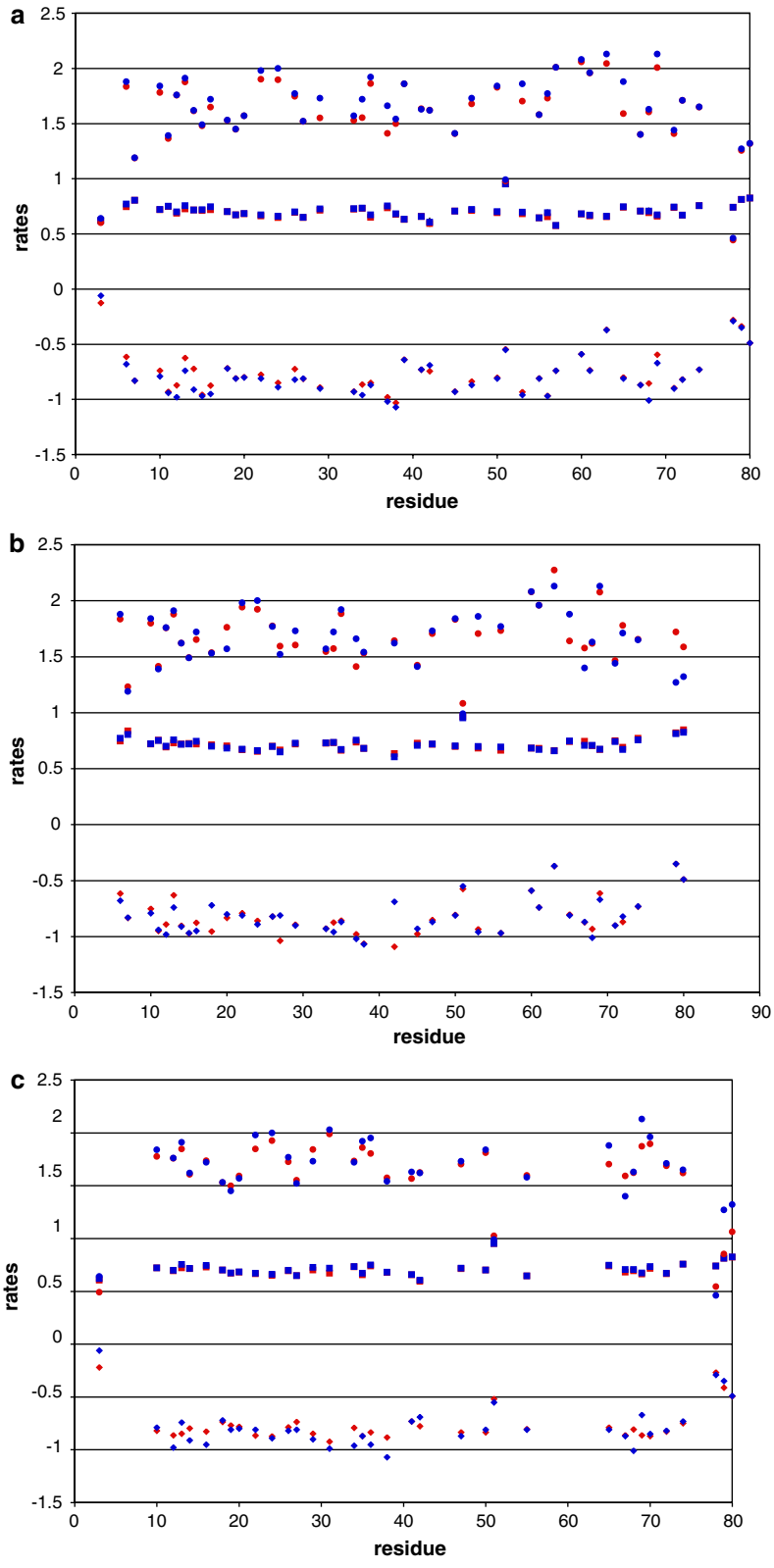
a
rates
residue
b
rates
residue
c
rates
residue

Table 1. Statistics of fitting the experimental relaxation data of calmodulin residues 1–80 using different parameters and variables

S^2	Θ (degree)	τ_{local} (ps)	τ_c (ns)	Number conv[a].	R_1 % error of fit[b]	$\eta_{xy}^{CO,COC\alpha}$ % error of fit	$\eta_{xy}^{CO,CON}$ % error of fit
var	var	var	6.9	47/56	1.0	2.8	4.6
0.76	var	var	6.9	30/56	0.6	5.4	7.0
var	*154*	*var*	*6.9*	*26/56*	*0.9*	*5.8*	*7.8*
var	*var*	*52*	*6.9*	*1/56*	–	–	–
var	*var*	*690*	*6.9*	*40/56*	*1.6*	*4.5*	*5.5*
var	dCOCα[c]	var	6.9	35/56	1.2	4.8	8.2
var	var	var	6.9/6.5[d]	100/104	1.2	3.1	3.5
var[e]	var	var	4.15	62/64	1.4	1.6	7.6

The fixed parameters in rows 2–5 (in italics) correspond to the averages found for the unrestrained fitting (row 1). [a]The number of converged residues divided by the number for of residues for which complete data was available. [b]The % fit is defined as the average of $\frac{\sqrt{(x^{exp}-x^{fit})^2}}{\frac{1}{N}\sum x^{exp}} \times 100$. [c]The angle Θ was kept at 154 degrees, while the distance COCα was varied between 1.50 and 1.55 Å. [d] τ_c was 6.9 ns for residues 1–80, 6.5 ns for residues 81–148. [e]Results for the data of ubiquitin (see text).

As a final critical test, we also investigated whether the data can be fitted with S^2, τ_{loc} and *another* variable, namely the distance $^{13}CO - ^{13}C\alpha$, bracketed between 1.50 and 1.55 Å. This range corresponds to the range seen in the ultra-high resolution (0.54 Å) X-ray structure of Crambin at 77°K (Jelsch et al., 2000). Figure 6c and Table 1 show that the data cannot be fitted by these three parameters nearly as well as by using a variable theta (see also Table 1).

In summary, the accuracy simulations strongly indicate, that good fits can *only* be obtained with reasonable values of σ_{11}, σ_{33} and τ_c. Change of any of these parameters results in significantly worse fits. The fitting strongly indicates that the three parameters S^2, τ_{loc} and Θ vary from residue to residue. Keeping any of these fixed cannot generate a decent fit either. Neither can the choice of another fitting variable, for instance, the distance COCα. Hence, the ^{13}CO relaxation data are affected by S^2, τ_{loc} and Θ, and fitting with them is necessary and sufficient.

What do the fitted parameters mean?

The different ^{13}CO relaxation rates R_1^{CO}, $\eta_{xy}^{CO,COC\alpha}$ and $\eta_{xy}^{CO,CON}$ used herein report on the global and local motions of different magnetic relaxation vectors. As in classical Model Free theory, the global motion should be (nearly) isotropic for the theory to be valid (Lipari and Szabo, 1982a). The local motions may or may not be isotropic. In the latter, more common case, the local motions affecting the different magnetic vectors contributing to the ^{13}CO relaxation must, at least in principle, be described by different order parameters.

In the following, we describe the dependency of the different relaxation mechanisms on rotational fluctuations around three imaginary axes: following (Bremi and Bruschweiler, 1997) we define the vector linking the two Cα atoms adjacent to the peptide plane as the rotational axis as γ, a vector perpendicular to the peptide plane as β, and a vector perpendicular to γ and β as α. As is seen in Figure 7, α, β and γ are nearly parallel to the σ_{22}, ^{13}CO-CSA and NH dipolar relaxation vectors, the σ_{33} ^{13}CO-CSA relaxation vector and the $^{13}CO - ^{13}C\alpha$ dipolar and σ_{11} ^{13}CO-CSA relaxation vectors, respectively.

In large molecules, the *dipolar* component of the R_1^{CO} relaxation is completely dominated by $^{13}CO - ^{13}C\alpha$ relaxation, mostly due to the fact that the latter is in turn dominated by $J(0)$. Hence, the dipolar R_1^{CO} relaxation is only sensitive to fluctuations around axes perpendicular to the $^{13}CO - ^{13}C\alpha$ direction, i.e. axial fluctuations around α and β. This behavior is plotted in Figure 7 which was computed using equations (2) to (7). Details of these and the following computations are given in the Supplementary Material.

The R_1^{CO} relaxation of the non-axially symmetric ^{13}CO CSA will be most efficient upon motions in which the "largest" (σ_{11}) and "smallest" (σ_{33}) axes are fully interchanged with respect to the external field, i.e. a motion around σ_{22}, or an "α" motion. Like the dipolar R_1^{CO} relaxation, γ motions are not very effective.

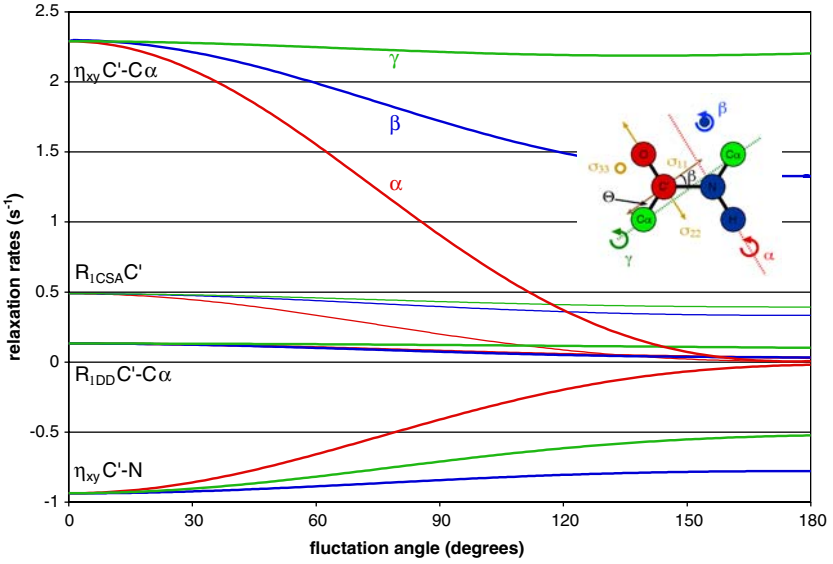

Figure 7. Computations of the dependence of different relaxation mechanisms upon local fluctuations around the different axes α, β and γ of the peptide plane as defined in the insets. Parameters used: $\tau_c = 6.9$ ns, $\tau_{local} = 0$, $\sigma_{11} = 270$, $\sigma_{22} = 165$ and $\sigma_{33} = 84$ ppm, $B_0 = 11.76$ Tesla. See the supplemental materials for more information.

The $\eta_{xy}^{CO,COC\alpha}$ cross correlated relaxation, dependent on similar terms as the CSA R_1^{CO} relaxation, shows a similar dependence on the axial fluctuations as the CSA R_1^{CO} as is demonstrated in Figure 7.

The $\eta_{xy}^{CO,CON}$ is seen in Figure 7 to be dominated by motions around the α axis, with β and γ being relatively inefficient.

Hence, all (major) relaxation mechanisms contributing to the effective "order parameter" S^2_{CO} to which COMFORD fits the three relaxation rates, have *in common* that they are most sensitive to fluctuations about α, and least sensitive to motions about γ, the so-called crankshaft motion (Fadel et al., 1995) (see Figure 7).

These predictions were put to the test as follows. We computed relaxation rates for varying amounts of pure alpha, beta or gamma local motions at a range of time scales, using the orientational-dependent order parameters listed in the Appendix. Subsequently, we fitted the rates back with COMFORD and compared the effective COMFORD S^2_{CO} with the input order parameters S^2_{alpha}, S^2_{beta} and S^2_{gamma}. The results in Figure 8(a–c) respectively, show, indeed, that effective S^2_{CO} follows S^2_{alpha} quite closely, while it hardly detects the decrease in S^2_{beta} or S^2_{gamma}. Figure 8d shows how well COMFORD fits to the timescale (τ_{loc}) of pure α motion. The combined tests in Figure 8 thus confirm the predictions of Figure 7, and establish the effective COMFORD S^2_{CO}, with the effective τ_{loc}, as reliable measure of the amount and timescale of α-type fluctuations contained in the local motion.

In contrast, the commonly measured relaxation of the NH vector is, obviously, insensitive to motions about α, being parallel to that bond direction, while most sensitive to fluctuations about β and γ both perpendicular to that bond direction (not shown). Consequently, when comparing conventional S^2_{NH} order parameters with the effective S^2_{CO} order parameter, the following guidelines hold: when for a region S^2_{NH} is smaller than the median value $< S^2_{NH} >$, while S^2_{CO} is equal to $< S^2_{CO} >$, γ-type motions are implied; when for a region S^2_{NH} is equal to $< S^2_{NH} >$, while S^2_{CO} is smaller than $< S^2_{CO} >$, α-type motions are implied; when for a particular region both S^2_{NH} is smaller than $< S^2_{NH} >$, and S^2_{CO} is smaller than $< S^2_{CO} >$, isotropic local motions are implied.

The above argumentation is valid only if the peptide plane, and all of its connected vectors, is planar and rigid. This is certainly correct for vectors involving the atoms Cα(i), C(i), O(i) and N(i + 1). However, there is both experimental and theoretical evidence that the NH bond vector can

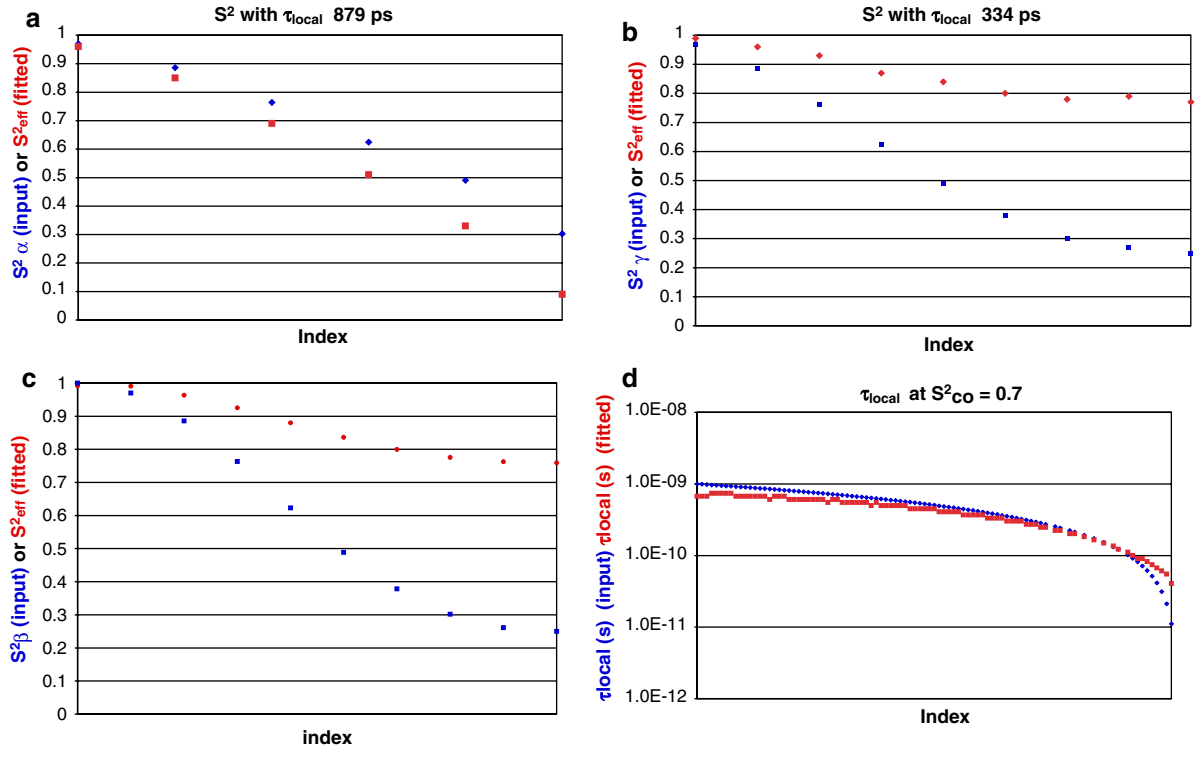

Figure 8. Panel A: COMFORD fitting of the effective S^2_{CO} (red) vs. S^2_{alpha} (pure alpha motion) (blue), with $\tau_{local} = 880$ ps. Panel B: COMFORD fitting of the effective S^2_{CO} (red) vs. S^2_{beta} (pure beta motion) (blue), with $\tau_{local} = 670$ ps. Panel C: COMFORD fitting of the effective S^2_{CO} (red) vs. S^2_{gamma} (pure gamma motion) (blue), with $\tau_{local} = 880$ ps. Panel D: COMFORD fitting of the effective τ_{local} (red) vs. $\tau_{local_{alpha}}$ (pure alpha motion) (blue), with $S^2_{alpha} = 0.70$.

deviate significantly from the peptide plane through nitrogen pyramidalization (statically up to 11 degrees; Ulmer et al., 2003; dynamically up to 30 degrees Palmo et al., 2003; Mannfors et al., 2003). Consequently, the motions of the ^{13}CO and NH relaxation vectors are not strictly correlated. In this respect, the ^{13}CO relaxation paradigm may actually give better insight in the peptide backbone dynamics than the NH vector dynamics.

Comparison with NH dynamics

Calmodulin

Our studies were carried out with the small protein Calmodulin (16 kDa). The protein consists of two EF hand domains, residues 1–77 and 82–148, respectively. The two domains are connected by a flexible linker between the residues 77–81 and the overall structure is best described as two (almost) independently diffusing EF hand domains connected by a string. For this study we assume that the domains diffuse isotropically, with a correlation time of 6.9 ns for the N-terminal, and 6.5 ns for the C-terminal domain, as was determined from ^{15}N relaxation experiments as well as by optimization of fitting the ^{13}CO experiments.

Figure 9 presents the raw and fitted relaxation data for all residues of Calmodulin. The fits are seen to be excellent. Figure 10(a, b) compare the fitted ^{13}CO relaxation parameter S^2_{CO} with the related parameters for the ^{15}N relaxation. The comparison of both measures of dynamics yields more correspondences than differences. For instance, both methods detect flexibility in the central linker between the two domains (residues 77–81), and the motions of the N and C-terminus. Salient differences are seen for residues 85–91 and 115–135. Here, the S^2_{NH} parameters fluctuate around the average values (0.85) while the S^2_{CO} parameters are

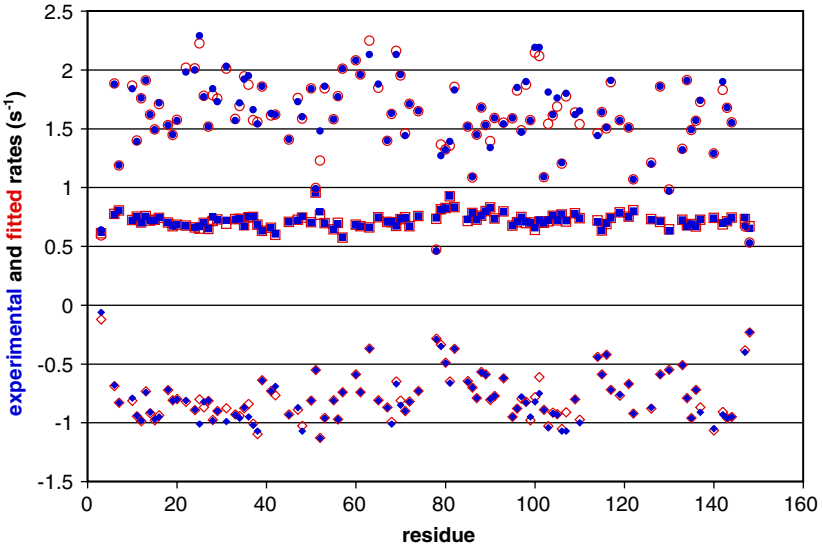

Figure 9. Fitting of the relaxation rates of all residues of Ca^{2+}-saturated Calmodulin (600 MHz). The fitting took into account that residues 1–80 are best described with $\tau_c = 6.9$ ns, while residues 81–148 are best characterized with $\tau_c = 6.5$ ns. Other parameters were $\sigma_{11} = 245$ ppm, and $\sigma_{33} = 93$ ppm for the ^{13}CO CSA. The experimental and fitted $\eta_{xy}^{CO,COC\alpha}$ are in blue and red *circles* respectively. The experimental and fitted R_1^{CO} are in blue and red *squares* respectively. The experimental and fitted $\eta_{xy}^{CO,CON}$ are in blue and red *diamonds* respectively. Error bars are shown for the experimental data only.

significantly lower than their mean value. Hence, these regions indicate the presence of anisotropic motions of the α-type.

Ubiquitin

A COMFORD analysis was carried out on the relaxation data available for ubiquitin from the supplementary materials presented by (Loth et al., 2005). By optimization of the fitting, we obtained a τ_c of 4.15 ns (303 K) in good agreement with literature data. Figure 11 presents the raw and fitted relaxation data. The fits are seen to be excellent (see also Table 1), but this could only be achieved by doubling the reported experimental uncertainties; with the quoted experimental errors we could only fit 34 residues. In Figure 12(a, b), we compare the fitted ^{13}CO relaxation parameters S^2_{CO} with the related parameters for the ^{15}N relaxation. The latter were obtained from earlier work on Ubiquitin in our lab (Wang et al., 2003). Here, both measures of dynamics yield almost identical profiles.

Order parameter magnitude

In addition to the local differences and correspondences described above, there are significant qualitative differences between S^2_{CO} and S^2_{NH} for Calmodulin, for Ubiquitin, and between them. For Calmodulin, $< S^2_{CO} >_{6-145} = 0.74$ is significantly smaller than $< S^2_{NH} >_{6-145} = 0.81$ (Figure 10a, b). Surprisingly, we find the exact *opposite* for ubiquitin: $< S^2_{CO} >_{4-68} = 0.95$ is significantly larger than $< S^2_{NH} >_{5-71} = 0.82$ (Figure 12a, b). Initially we considered that the difference should be ascribed to the fact that $< S^2_{CO} >$ (Figure 12a; Loth et al., 2005 data, our analysis) and $< S^2_{NH} >$ (Figure 12b; Wang et al., 2003 data, our analysis) were derived from different protein preparations in different labs. To investigate the difference, we also computed an approximate order parameter S^2_{NH} for ubiquitin from the available R_1^{NH}, $^1H \rightarrow {}^{15}N$ NOE and $\eta_{xy}^{N,NH}$ data (no R_2^{NH} data was given, Loth et al., 2005) using an in-house written program. That profile is shown in Figure 12c. It is apparent that Figure 12(b, c) correspond closely ($< S^2_{NH} >_{5-71} = 0.82$ for both) so that we conclude that the difference between the average order parameters in Figure 12(a–c) is genuine.

Timescale of the local motions

For calmodulin, we obtain a $< \tau_{local}^{CO} >$ of 550 ps which is substantially larger than the $< \tau_{local}^{NH} >$ of 60 ps (see Figure 10c). There is nothing in relaxa-

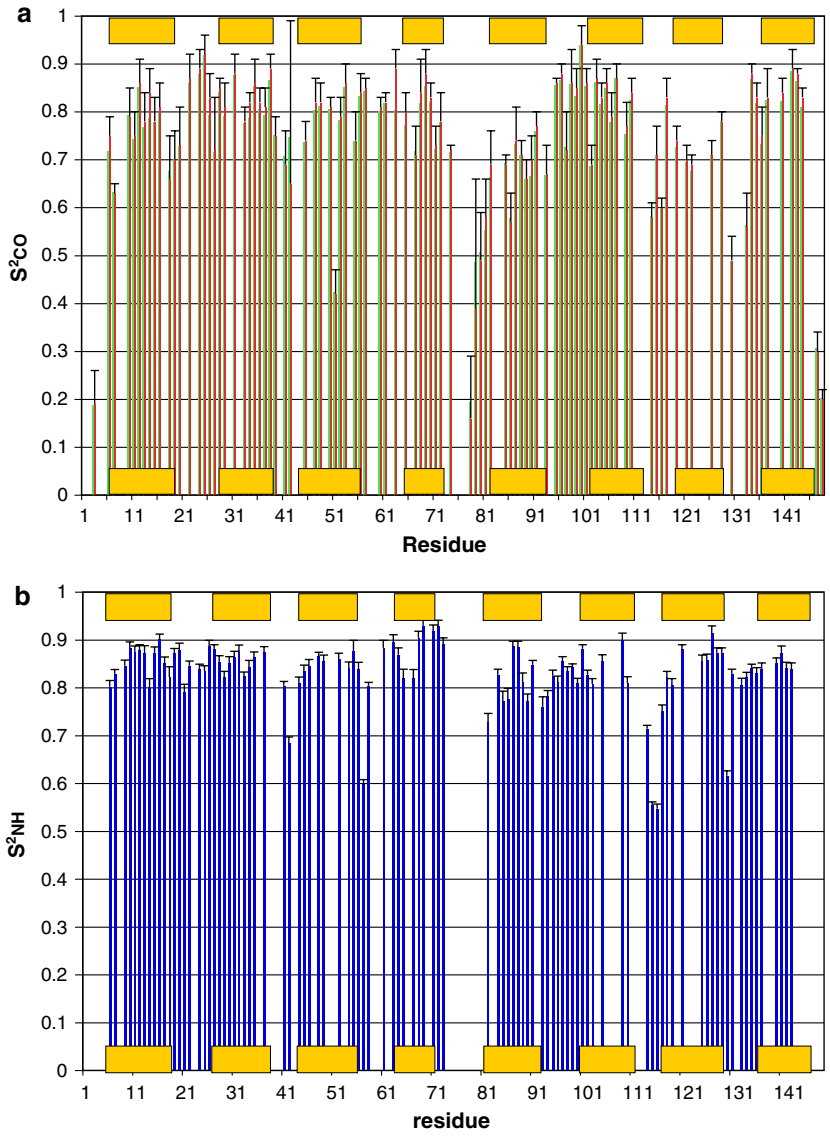

Figure 10. Comparison of the fitted ^{13}CO and ^{15}N NH Lipari–Szabo parameters for Ca^{2+} saturated calmodulin. a) The fitted S^2_{CO} order parameters, in green the averages of the calculations, in red the peak values with errors (see explanation at Figure 4). b) the conventional S^2_{NH} order parameters (Mandel et al., 1995). c) The fitted τ_{local} associated with the S^2_{CO} parameters are in red circles; the τ_{local} associated with the S^2_{NH} parameters are in blue squares. d) The secondary structure (helices) is indicated with yellow boxes.

tion theory that makes the $^{13}CO - ^{13}C\alpha$ vector intrinsically more sensitive to slower motions than the NH vector. Hence, the differences suggest that there are real differences in the time scales of the motions that are detected by the different relaxation mechanisms. Remarkably, the τ^{CO}_{local} rather faithfully traces the Calmodulin secondary structure: the rates are typically slow in helices and fast in the loops. These trends are also visible for the τ^{NH}_{local}, but interestingly, there the local correlation time increases when approaching the break in the central helix. It would be reasonable to expect that the NH vector in helices mostly monitors fast motions of the hydrogen atom in the combined forcefield of valences and hydrogen bonding, whereas the $^{13}CO - ^{13}C\alpha$ vectors report on slower motions of heavier molecular fragments. In loops, the motional freedom of both vectors becomes comparable.

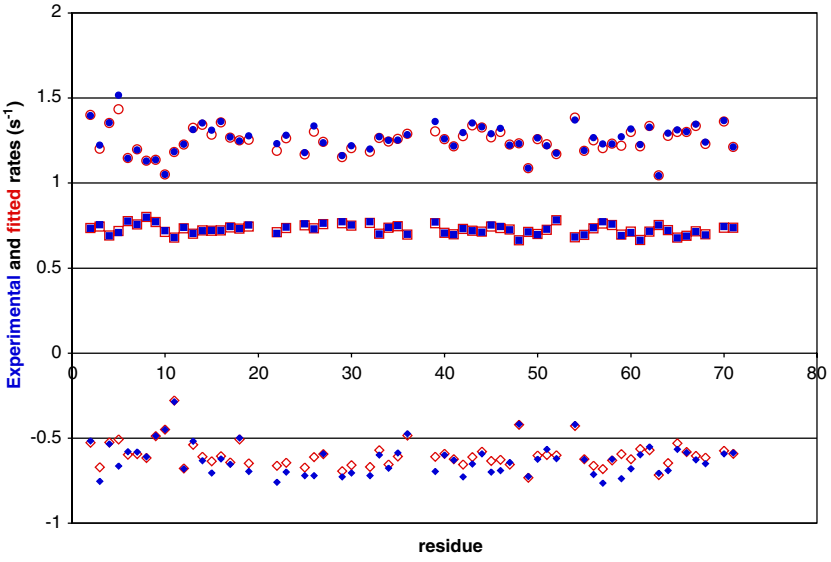

Figure 11. Fitting of the relaxation rates of human ubiquitin at 303 K. The data were obtained from the supplementary material provided by (Loth et al., 2005). The fitting converged best with a value of $\tau_c = 4.15$ ns, $\sigma_{11} = 245$ ppm, and $\sigma_{33} = 93$ ppm. The value of σ_{22} was obtained from $\sigma_{22} = \sigma_{iso} * 3 - \sigma_{11} - \sigma_{33}$. The experimental and fitted $\eta_{xy}^{CO,COC\alpha}$ are in blue and red *circles* respectively. The experimental and fitted R_1^{CO} are in blue and red *squares* respectively. The experimental and fitted $\eta_{xy}^{CO,CON}$ are in blue and red *diamonds* respectively.

For ubiquitin, we find a $<\tau_{local}^{CO}>$ of 500 ps which is also substantially larger than the $<\tau_{local}^{NH}>$ of 42 ps (see Figure 12c). It seems significant that the best fit of fourteen relaxation experiments for ubiquitin (Loth et al., 2005), requires slow (400 ps) fluctuations of the peptide plane about the α-axis, in complete agreement with our findings.

^{13}CO CSA tensor orientation

The COMFORD fitting of the angle Θ of the σ_{11} axis of the ^{13}CO CSA tensor with respect to the COCα bond vector, yields an average of 153.8 degrees for Calmodulin and 154.6 for ubiquitin (the angle β of the σ_{11} axis with respect to the CON bond vector is 36.8 and 37.6 degrees respectively). These values are very close to the average value of 154.43 degrees as obtained for ubiquitin by (Loth et al., 2004) and the average found from DFT calculations (Marckwick and Sattler, 2004).

Figure 13 shows the variations in the angle Θ for both proteins. The spread of values is larger for calmodulin (rmsd = 8.8°) than for ubiquitin (rmsd = 4.8°), which, in turn, is larger than the spread in angles as obtained by the (Loth et al., 2005) analysis of the 14 cross and auto-correlation rates (rmsd 3.25°). COMFORD fitting yields outliers (Θ > 170 degrees and Θ < 140 degrees), both in Calmodulin and ubiquitin, that are not seen in the (Loth et al., 2005) analysis. The outliers occur in areas with extremely low order parameters. At present, we can not be certain whether these outliers are the consequence of an unfortunate S^2/Θ parameter interaction in the fitting procedure or if they are the consequence of the extreme dynamics yielding exceptional (dynamically averaged) atomic parameters.

The tensor angles obtained by COMFORD from the data of Loth et al (2005) do correlate with those reported by the (Loth et al., 2005) analysis. However, as the correlation plot in Figure 13c shows, the slope of the correlation line departs strongly from unity. These issues require more investigation.

Conclusion

The COMFORD program achieves excellent fits to the composite experimental NMR relaxation data $R_1^{CO}, \eta_{xy}^{CO,COC\alpha}$ and $\eta_{xy}^{CO,CON}$ of both

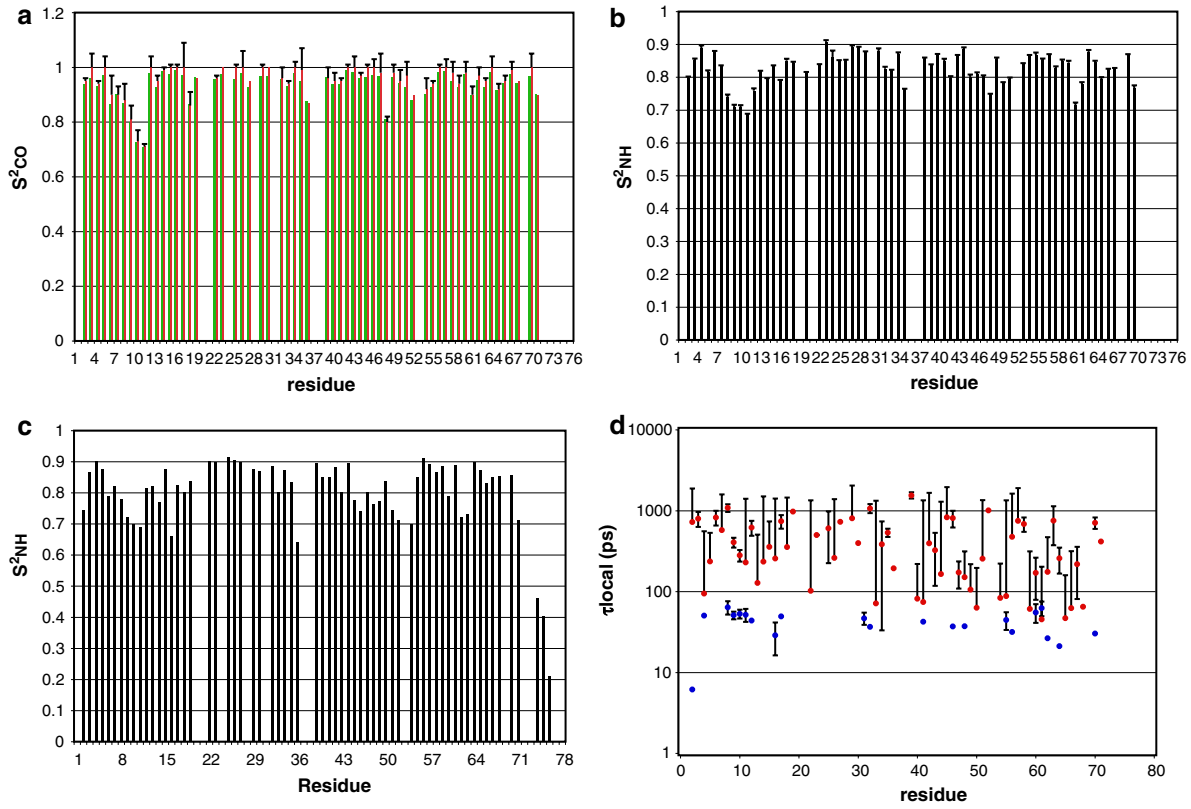

Figure 12. Comparison of the fitted ^{13}CO and ^{15}N NH Lipari–Szabo parameters for human ubiquitin. (a) The S^2_{CO} order parameters extracted with COMFORD from the R_1^{CO}, $\eta_{xy}^{CO,COC\alpha}$ and $\eta_{xy}^{CO,CON}$ data available from (Loth et al., 2005). In green are the averages of the calculations, in red the peak values with errors (see explanation at Figure 4). (b) the conventional S^2_{NH} order parameters extracted with MODELFREE (Mandel et al., 1995) from the R_2^{NH}, R_1^{NH} and $^1H \rightarrow {}^{15}N$ NOE data available from (Wang et al., 2003). (c) approximate S^2_{NH} order parameters extracted with in-house written code from the R_1^{NH}, $^1H \rightarrow {}^{15}N$ NOE and $\eta_{xy}^{N,NH}$ data available from (Loth et al., 2005) (no R_2^{NH} data was given) d) The fitted τ_{local} associated with the S^2_{CO} parameters are in red circles; the τ_{local} associated with the S^2_{NH} parameters (from MODELFREE) are in blue circles.

Calmodulin and Ubiquitin, when a minimum of three variables, S^2_{CO}, τ_{loc} and Θ are used with reasonable ranges and when sensible choices for atomic parameters and CSA-tensor values are made. The resulting fitted variables S^2_{CO}, τ_{loc} and Θ fall in ranges that are reasonable. Detailed analysis shows interesting differences between the ^{13}CO and ^{15}N relaxation paradigms: the composite ^{13}CO relaxation is particularly insensitive to fluctuations around the crank-shaft motion axis, while the NH relaxation is particularly insensitive to fluctuations around the perpendicular NH axis. Both are sensitive to fluctuations around an axis perpendicular to the peptide plane and to composite local motions. These different sensitivities can be used to distinguish motional models for the protein backbone. The fitting with COMFORD suggest that local motions in areas of secondary structure detected by the ^{13}CO vector are slower than those seen by the NH vector. The time scale of local motions in flexible loop areas as detected by both methods are similar.

Figure 13. The fitted angles Θ for the orientation of the ^{13}CO CSA tensor principal axis σ_{11} with respect to the CO – Cα bond vector for (a) Ca^{2+} saturated Calmodulin and (b) human ubiquitin. In (b) the Θ values extracted from the data of (Loth et al., 2005) using COMFORD (red circles) are compared with the values as presented by (Loth et al., 2005) with their isotropic model (blue squares). Panel c shows the correlation of the results in b; the data can be fitted by linear regression with $y = 0.51x + 76$, with a R^2 of 0.59.

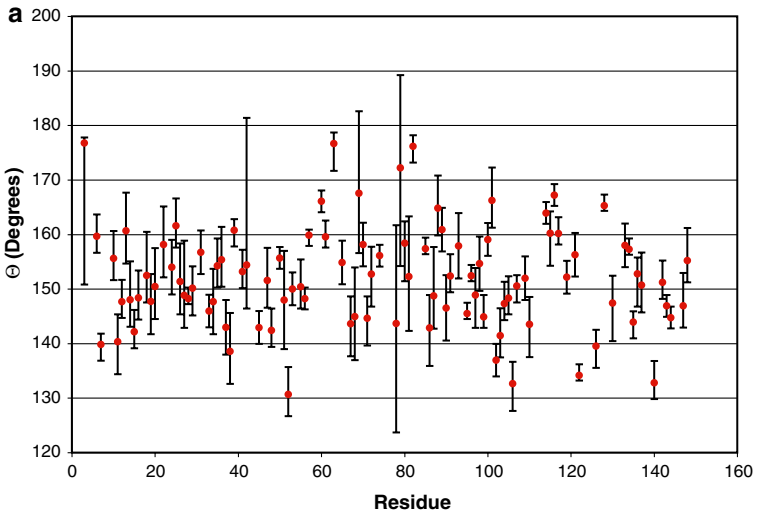
a
Θ (Degrees)
Residue
200
190
180
170
160
150
140
130
120
0
20
40
60
80
100
120
140
160

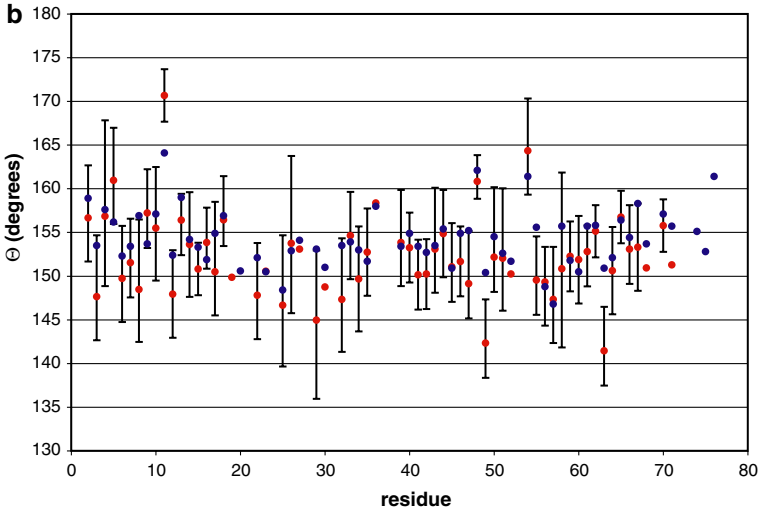
b
Θ (degrees)
residue
180
175
170
165
160
155
150
145
140
135
130
0
10
20
30
40
50
60
70
80

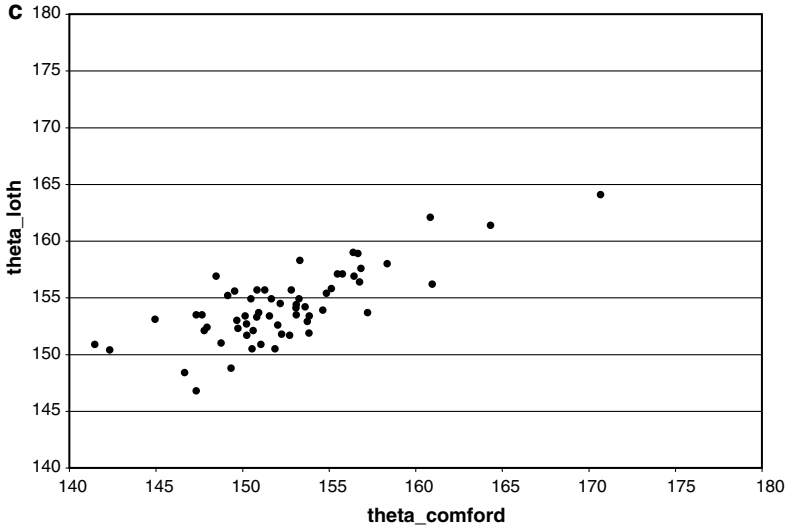
c
theta_loth
theta_comford
180
175
170
165
160
155
150
145
140
140
145
150
155
160
165
170
175
180

Acknowledgements

This work was supported by the National Science Foundation grant MCB 0135330. The authors thank Dr. A. J. Wand for the sample of calcium-saturated calmodulin and the NSF, NIH and Michigan Tri-Corridor for support of the NMR instruments used.

Supplementary material

An appendix describing the calculation of the simulations in Figure 7 with additional figures showing the ^{13}CO CSA relaxation as a function of local correlation time and motional direction. The electronic supplementary material is available to authorized users in the online version of this article at http://www.dx.doi.org/10.1007/s10858-006-9047-4.

References

Akke, M., Bruschweiler, R. and Palmer, A.G. (1993) *J. Am. Chem. Soc.*, **115**, 9832–9833.
Andrec, M., Montelione, G.T. and Levy, R.M. (1999) *J. Magn. Reson.*, **139**, 408–421.
Bremi, T. and Bruschweiler, R. (1997) *J. Am. Chem. Soc.*, **119**, 6672–6673.
Chang, S.L. and Tjandra, N. (2005) *J. Magn. Reson.*, **174**, 43–53.
Cisnetti, F., Loth, K., Pelupessy, P. and Bodenhausen, G. (2004) *Chem. PhysChem.*, **5**, 807–814.
Clore, G.M., Szabo, A., Bax, A., Kay, L.E., Driscoll, P.C. and Gronenborn, A.M. (1990) *J. Am. Chem. Soc.*, **112**, 4989–4991.
Cordier, F., Caffrey, M., Brutscher, B., Cusanovich, M., Marion, D. and Blackledge, M. (1998) *J. Mol. Biol*, **281**, 341–361.
Daragan, V.A. and Mayo, K.H. (1996) *J. Magn. Reson. B*, **110**, 164–175.
Daragan, V.A. and Mayo, K.H. (1997) *Progr. Nucl. Magn. Reson. Spectr.*, **31**, 63–75.
Dayie, K.T. and Wagner, G. (1997) *J. Am. Chem. Soc.*, **119**, 7797–7806.
Delaglio, F., Grzesiek, S., Vuister, G.W., Zhu, G., Pfeifer, J. and Bax, A. (1995) *J. Biomol. NMR*, **6**, 277–293.
D'Auvergne, E.J. and Gooley, P.R. (2003) *J. Biomol. NMR*, **25**, 25–39.
Dellwo, M.J. and Wand, A.J. (1989) *J. Am. Chem. Soc.*, **113**, 4571–4578.
Engelke, J. and Ruterjans, H. (1997) *J. Biomol. NMR*, **9**, 63–78.
Fadel, A.R., Jin, D.Q., Montelione, G.T. and Levy, R.M. (1995) *J. Biomol. NMR*, **6**, 221–226.
Farrow, N.A., Zhang, O., Szabo, A., Torchia, D.A. and Kay, L.E. (1995) *J. Biomolm. NMR*, **6**, 153–162.
Fischer, M.W.F., Zeng, L., Pang, Y., Hu, W., Majumdar, A. and Zuiderweg, E.R.P. (1997) *J. Am. Chem. Soc.*, **119**, 12629–12642.
Fischer, M.W., Zeng, L., Majumdar, A. and Zuiderweg, E.R.P. (1998a) *Proc. Natl. Acad. Sci. USA*, **95**, 8016–8019.
Fischer, M.W.F., Majumdar, A. and Zuiderweg, E.R.P. (1998b) *Progr. NMR Spectrosc.*, **33**, 207–272.
Ghose, R., Huang, K. and Prestegard, J.H. (1998) *J. Magn. Reson.*, **135**, 487–499.
Goldman, M. (1984) *J. Magn. Reson.*, **60**, 437–452.
Gu, Z., Zambrano, R. and McDermott, A. (1994) *J. Am. Chem. Soc.*, **116**, 6368–6372.
Ishima, R., Louis, J.M. and Torchia, D.A. (1999) *J. Magn. Reson.*, **137**, 289–292.
Ishima, R., Baber, J., Louis, J.M. and Torchia, D.A. (2004) *J. Biomolm. NMR*, **29**, 187–198.
Jelsch, C., Teeter, M.M., Lamzin, V., Pichon-Pesme, V., Blessing, R.H. and Lecomte, C. (2000) *Proc. Natl. Acad. Sci. USA*, **97**, 3171–3176.
Johnson, B.A. and Blevins, R.A. (1994) *J. Biomol. NMR*, **4**, 603–614.
Kay, L.E., Torchia, D.A. and Bax, A. (1989) *Biochemistry*, **28**, 8972–8979.
Kay, L.E., Muhandiram, D.R., Wolf, G., Shoelson, S.E. and Forman-Kay, J.D. (1998) *Nat. Struct. Biol.*, **5**, 156–163.
Lee, A.L., Kinnear, S.A. and Wand, A.J. (2000) *Nat. Struct. Biol.*, **7**, 72–77.
Levy, R.M., Karplus, M. and Wolynes, P.G. (1981) *J. Am. Chem. Soc.*, **103**, 5998–6011.
Lipari, G. and Szabo, A. (1982a) *J. Am. Chem. Soc.*, **104**, 4546–4558.
Lipari, G. and Szabo, A. (1982b) *J. Am. Chem. Soc.*, **104**, 4559–4570.
Loria, J.P., Rance, M. and Palmer, A.G. (1999) *J. Am. Chem. Soc.*, **121**, 2331–2332.
Loth, K., Pelupessy, P. and Bodenhausen, G. (2005) *J. Am. Chem. Soc.*, **127**, 6062–6068.
Mandel, A.M., Akke, M. and Palmer, A.G. III (1995) *J. Mol. Biol.*, **246**, 144–163.
Mannfors, B.E., Mirkin, N.G., Palmo, K. and Krimm, S. (2003) *J. Phys. Chem. A*, **A107**, 1825–1832.
Markwick, P.R. and Sattler, M. (2004) *J. Am. Chem. Soc.*, **126**, 11424–11425.
Orekhov, V.Y., Pervushin, K.V. and Arseniev, A.S. (1994) *Eur. J. Biochem.*, **219**, 887–896.
Palmo, K., Mannfors, B., Mirkin, N.G. and Krimm, S. (2003) *Biopolymers*, **68**, 383–394.
Pang, Y.X. and Zuiderweg, E.R.P. (2000) *J. Am. Chem. Soc.*, **122**, 4841–4842.
Pang, Y.X., Buck, M. and Zuiderweg, E.R.P. (2002) *Biochemistry*, **41**, 2655–2666.
Peng, J.W. and Wagner, G. (1992a) *J. Magn. Reson.*, **98**, 308–332.
Peng, J.W. and Wagner, G. (1992b) *Biochemistry*, **31**, 8571–8586.
Tjandra, N., Szabo, A. and Bax, A. (1996) *J. Am. Chem. Soc.*, **118**, 6986–6991.
Ulmer, T.S., Ramirez, B.E., Delaglio, F. and Bax, A. (2003) *J. Am. Chem. Soc.*, **125**, 9179–9191.
Urbauer, J.L., Short, J.H., Dow, L.K. and Wand, A.J. (1995) *Biochemistry*, **34**, 8099–8109.
Wang, T.-Z., Cai, S. and Zuiderweg, E.R.P. (2003) *J. Am. Chem. Soc.*, **125**, 8639–8643.
Wang, T.-Z., Frederick, K.K., Igumenova, T.I., Wand, A.J. and Zuiderweg, E.R.P. (2005) *J. Am. Chem. Soc.*, **127**, 828–829.
Yang, D., Mok, Y.K., Forman-Kay, J.D., Farrow, N.A. and Kay, L.E. (1997) *J. Mol. Biol.*, **272**, 790–804.
Yang, D., Mittermaier, A., Mok, Y.K. and Kay, L.E. (1998) *J. Mol. Biol.*, **276**, 939–954.
Zeng, L., Fischer, M.W.F. and Zuiderweg, E.R.P. (1996) *J. Biomol. NMR*, **7**, 157–162.